REPUBLIQUE ALGERIENNE DEMOCRATIQUE ET POPULAIRE

MINISTERE DE L'ENSEIGNEMENT SUPERIEUR ET DE LA RECHERCHE SCIENTIFIQUE

UNIVERSITE MOHAMED BOUDIAF - M'SILA

FACULTE DE TECHNOLOGIE

DEPARTEMENT D'ELECTRONIQUE

N° : ………/Dept. Electronique/2023

1985

جامعة محمد بوضياف - المسيلة

Université Mohamed Boudiaf - M'sila

DOMAINE : SCIENCE ET TECHNOLOGIE

FILIERE : ELECTRONIQUE

OPTION : ELECTRONIQUE DES SYSTEMES EMBARQUES

Mémoire présenté pour l'obtention

Du diplôme de Master Académique

Par :

TAHAR CHEBABHI

AHMED MESSAAD

Intitulé

MY DAILY HEALTH
Helping system for medical diagnosis using artificial intelligence

Soutenu publiquement le 02 Juillet 2023 devant le jury composé de :

Mohamed LADJAL	Prof. / Univ. de M'sila	Président
Youcef BRIK	MCA / Univ. de M'sila	Encadrant
Ishaq AICHE	Doctorant / Univ. de M'sila	Co-Encadrant
Mohamed DJERIOUI	MCA / Univ. de M'sila	Examinateur
Aimen ZAYD	MCA / Univ. de M'sila	Représentant de l'incubateur
Zineelabidine RAHMOUNI	Prof. / Univ. de M'sila	Représentant du CATI
Dr.	Docteur Radiologue	Partenaire socio-économique
Dr.	Docteur Radiologue	Partenaire socio-économique

Année universitaire : 2022 / 2023

Acknowledgements

We are grateful to Allah for His guidance throughout this search.
We extend our heartfelt appreciation to our supervisors, Dr. Youcef BRIK and co-supervisor, Ishaq AICHE, for their invaluable guidance and support.
Our gratitude also goes to our families, friends, and the Electronics department for their unwavering support.
We would like to thank all the participants for their valuable contributions.
Thank you for your support throughout this journey.

Abstract:

This research focuses on the application of deep transfer learning in disease analysis using biomedical data. This research explores the application of deep transfer learning models, such as ResNet50, DenseNet-121, and EfficientNet-B3, in analyzing brain tumors, Alzheimer's disease, respiratory diseases, skin cancer, and gastrointestinal diseases.

Résumé:

Cette recherche se concentre sur l'application de l'apprentissage par transfert profond dans l'analyse des maladies à l'aide de données biomédicales. Cette recherche explore l'application de modèles d'apprentissage par transfert profond, tels que ResNet50, DenseNet-121 et EfficientNet-B3, dans l'analyse des tumeurs cérébrales, de la maladie d'Alzheimer, des maladies respiratoires, du cancer de la peau et des maladies gastro-intestinales.

ملخص :

يركز هذا البحث على تطبيق التعلم العميق للنقل في تحليل الأمراض باستخدام البيانات الطبية الحيوية. يستكشف هذا البحث تطبيق نماذج تعلم النقل العميق، مثل ResNet50 و DenseNet-121 وEfficientNet-B3 ، في تحليل أورام الدماغ ومرض الزهايمر وأمراض الجهاز التنفسي وسرطان الجلد وأمراض الجهاز الهضمي.

Contents

List of Tables

List of Figures

INTRODUCTION GENERAL

Artificial intelligence (AI) and biological data analysis have advanced significantly in recent years, providing new opportunities for disease diagnosis, treatment planning, and patient monitoring. Biomedical data, which includes a variety of medical imaging and clinical data, is crucial in revealing the complex mechanisms underlying different health disorders. The use of AI methods, especially deep learning and transfer learning, has emerged as a game-changing method for gleaning relevant information from this vast amount of biomedical data[1].

Biomedical data can be collected through various imaging techniques such as X-ray, PET, CT, microscopic, RGB, MRI, CT, and PET. Combining data from multiple modalities helps clinicians and researchers gain a better understanding of complex medical diseases, leading to more accurate diagnoses and treatment decisions.

AI involves developing computational systems for tasks traditionally requiring human intelligence. ML focuses on algorithms that enable computers to learn from data without explicit programming. Deep learning, a relevant ML subfield, autonomously extracts features and patterns from biomedical images. This improves disease characterization and diagnostic precision by revealing hidden structures. Transfer learning, a powerful method, addresses challenges in processing biomedical data by transferring knowledge from pre-trained models to enhance performance on smaller or specialized datasets with fewer data points[2].

This research specifically focuses on applying deep transfer learning in disease analysis using biological data. It provides a comprehensive review of cutting-edge methods for analyzing biomedical data related to brain tumors, Alzheimer's disease, respiratory illnesses, skin cancer, and gastrointestinal diseases. The study emphasizes the importance of deep transfer learning models such as ResNet50, DenseNet-121, and EfficientNet-B3, as well as the role of data augmentation techniques in enhancing their effectiveness. To provide empirical evidence, the study adopts an experimental approach that includes data description, evaluation metrics, and testing experiences. By comparing different parameters and evaluating the impact of data augmentation, the research unveils the efficacy and potential of deep transfer learning models in disease analysis. Moreover, it highlights practical applications and offers guidance on the optimal utilization of these methods in clinical settings.

The use of artificial intelligence, in particular deep transfer learning, to the study of biomedical data has enormous potential for improving patient care, illness detection, and therapy. Researchers and doctors can access a wealth of information by fusing advanced algorithms with large biomedical databases, resulting in more precise and effective illness analysis. In the long run, this interdisciplinary strategy has the potential to greatly enhance clinical results, increase our comprehension of complicated medical diseases, and influence the direction of healthcare.

Chapter 1

BIOMEDICAL DATA AND AI

1.1 Introduction

In recent times, the development and use of artificial intelligence (AI) in medicine has seen a surge due to the increasing number of computer hardware and software applications and the digitization of health data. This advancement poses new opportunities, challenges, and potential directions for AI in healthcare.

In this chapter, we will look at the biomedical data available today, and particularly focus on biomedical images. We will also explore AI and its capacity to play a major role in the healthcare sector.

1.2 Biomedical data

From the beginning, the concepts of illness and its treatment were intertwined with those of data observation and analysis. Whether we consider the illness descriptions and management instructions in early Greek literature or the current physician's utilization of complicated laboratory and X-ray tests, it is evident that data collection and interpretation are critical components of the health care process. As a result, a textbook on computers in biomedicine will frequently relate to data collecting, storage, and usage difficulties. This chapter establishes the groundwork for this repeating collection of concerns that are relevant to all elements of computer usage in biomedicine, both clinically and in applications connected to biology and human genetics.

Data are important to all medical treatment since they are critical to the decision-making process. In reality, a simple examination will demonstrate that all medical care actions include the collection, analysis, or use of data.

Data serve as the foundation for classifying a patient's issues or identifying subgroups within a patient population. They also assist a physician in determining what more information is required and what steps should be done to get a better understanding of a patient's situation or to treat the problem that has been identified most effectively [3].

1.3 BIOMEDICAL DATA TYPES

The term ”medical imaging” describes a variety of methods used to view particular body areas for use in clinical diagnosis and medical treatment. The functionality of a tissue or organ can also be visualized using medical imaging. With the use of medical imaging technology, doctors may look within the bones and skin to make diagnoses and administer treatment. Researcher-useable datasets for physiology and normal anatomy are also produced with the aid of medical imaging [4].

Medical imaging is a subset of the larger discipline of biological imaging, which encompasses a wide range of imaging methods, including

1.3.1 Magnetic Resonance Imaging (MRI)

Magnetic Resonance Imaging or MRI is a non-invasive means of mapping the interior structure of the body as well as some aspects of function. It employs nonionizing electromagnetic radiation and appears to pose minimal exposure risk. It generates high-quality cross-sectional pictures of the body in any plane by using radio frequency (RF) radiation in the presence of properly regulated magnetic fields. The MR image is created by putting the patient within a huge magnet that generates a reasonably high external magnetic field. This causes the nuclei of numerous atoms in the body, including hydrogen, to align with the magnetic field, and the RF signal to be applied later. Compute detects and uses energy emitted from the body to generate the MR picture [5], as indicated in Figure I.1 .

1.3.2 X-Ray imaging

X-rays use invisible electromagnetic energy beams to produce images of internal tissues, bones, and organs on film or digital media. They are used to diagnose tumors and bone injuries, and pass through body structures onto specially-treated plates or digital media. The more solid a structure is, the whiter it appears on the film.

When the body undergoes X-rays, different parts of the body allow varying amounts of

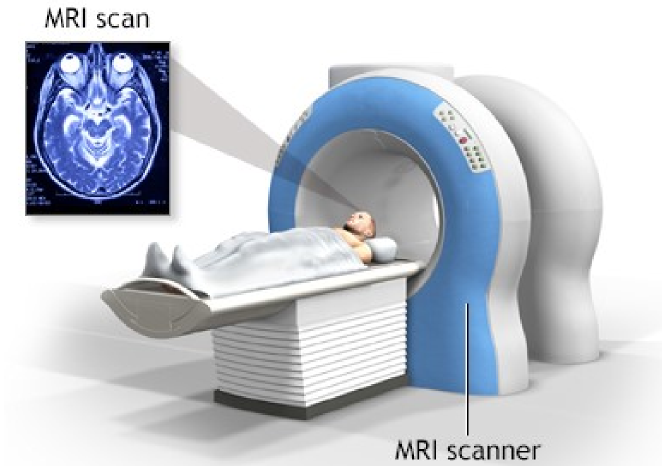

Figure 1.1: The magnetic resonance imaging (MRI) scanner

the X-ray beams to pass through. The soft tissues in the body (such as blood, skin, fat, and muscle) allow most of the X-ray to pass through and appear dark gray on the film or digital media. A bone or a tumor, which is more dense than soft tissue, allows few of the X-rays to pass through and appears white on the X-ray. When a break in a bone has occurred, the X-ray beam passes through the broken area and appears as a dark line in the white bone as showing in Figure I.2 [6].

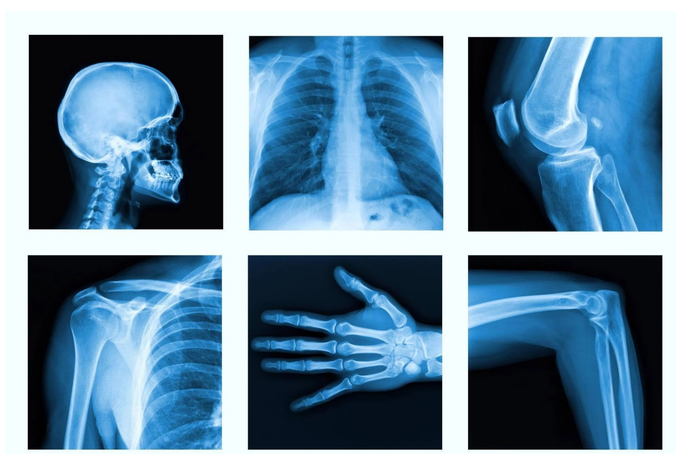

Figure 1.2: X-Ray images

1.3.3 PET images

Positron Emission Tomography (PET) involves injecting a radioactive tracer into the body, which emits positrons that travel a short distance in tissue before being annihilated with an electron, producing two photons of equal energy. PET scanners contain rings of scintillation detectors that register thousands of coincidence events per second, allowing the paths of the photons to be traced and the source of positron annihilation to be determined. This data is used to create a tomographic image using reconstruction software as indicated in Figure I.3.

PET uses a radioactive tracer to produce images of the body. When the tracer emits positrons, they travel a short distance before being annihilated with an electron, producing photons that are detected by a ring of scintillation detectors. The data from these detectors is used to determine the location of the source of positron annihilation and create a tomographic image [7].

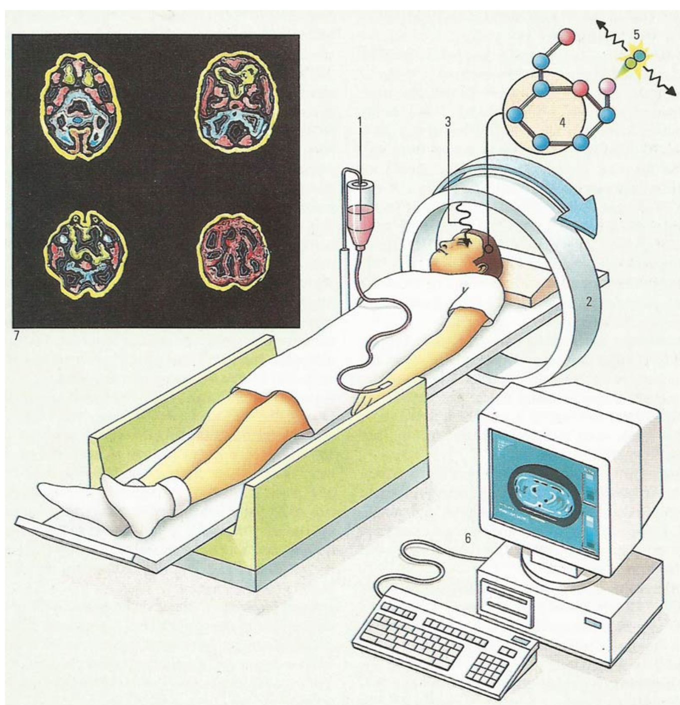

Figure 1.3: Positron emission tomography system

1.3.4 CT images

A computerized tomography (CT) scan is a diagnostic imaging process that creates images of the inside of the body using X-rays and computer technologies. In 1971, a patient's brain anatomy was first visualized with CT in the UK.

CT is a crucial diagnostic technology that is employed to assess a variety of medical disorders. Recent developments in CT technology include the extreme multidetector CT, iterative reconstruction techniques, dual-energy CT, cone-beam CT, portable CT, and phase contrast CT, all of which have already had or are anticipated to have a substantial therapeutic impact [8].

CT scans provide a high-resolution view of the body's internal compartments, such as adipose tissue, skeletal muscle, bones, and organs. Advanced CT technology allows for the accurate differentiation between the visceral and subcutaneous fat, as well as the cortical and trabecular bone, which is highly valuable in medical studies. The images also enable the detection of components within the subcutaneous adipose tissue, muscle and liver fat, as well as determining the attenuation and mineral density of skeletal muscle, which can be related to metabolic disorders. Accurate and reproducible measurements of the area and volume of each human body compartment can be obtained from CT scans, with the help of methods like manual planimetry, semi-automatic segmentation, stereological point-counting, and geometrical models[9].

1.3.5 Microscopic images

Microscopic images are magnified images of small objects that are too small to be seen with the naked eye. These images are usually captured using a microscope, which magnifies the object by a factor of 10 to 1000 times, allowing the viewer to see intricate details. Microscopic images can be used to observe a range of biological objects, including cells, bacteria, viruses, and other small organisms.

They can also be used to view non-biological specimens, such as crystals and minerals. Microscopic images are invaluable for scientists and medical professionals, as they allow

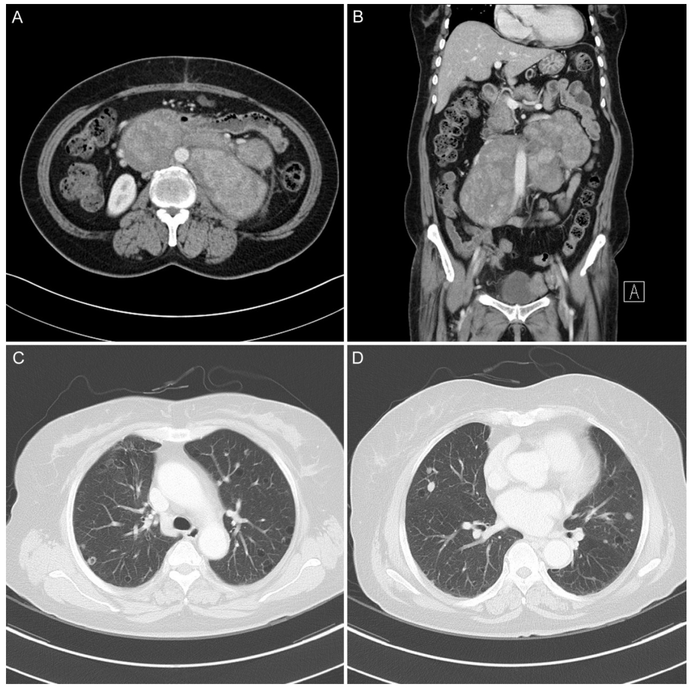

Figure 1.4: Computerized tomography (CT)

for detailed analysis of the observed objects.

1.3.6 RGB data pictures (Retinal)

Healthcare professionals in this manner take RGB photographs of the organs the patient requires. Typically, a high-precision camera or a microscope is used to capture these images. a crucial imaging technique for examining the interior organization of organs like the eye. It is mostly utilized as a non-invasive, quicker way to detect pathological or physiological changes in the retina.

These pictures were taken with a fundus camera that works on the basis of two monocular images. As seen in Figure I.6, retinal fundus scans are acquired under the direction of specialists to look for abnormalities within the retina [10].

Diabetic Retinopathy (DR) is a serious medical condition in which the blood vessels of the retina become damaged, leading to the leakage of fluids and blood. This damage can cause severe vision loss if left untreated and is the leading cause of blindness in diabetes patients. Early diagnosis of DR is essential, and regular retina screenings are key to

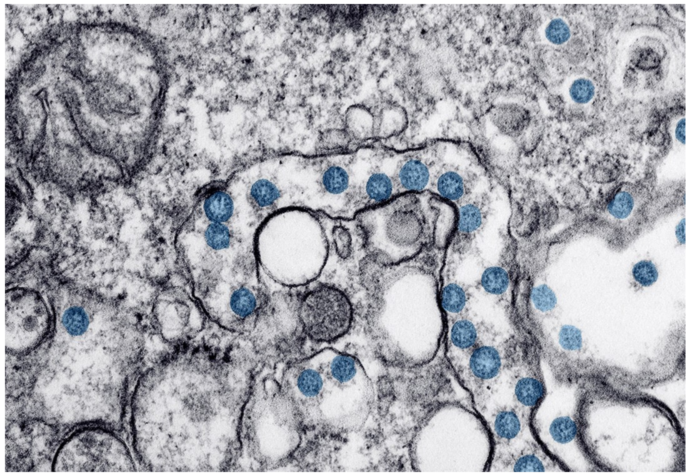

Figure 1.5: blog-coronavirus-vail

identify the condition at an early stage. DR is characterized by the emergence of various types of lesions on a retina scan, such as microaneurysms (MA), haemorrhages (HM), and soft and hard exudates (EX). Treatment options vary but may include laser therapy, medication, and surgery.

1.3.7 Other data images

Ultrasound: High-frequency sound waves are used in ultrasound imaging, also known as sonography, to view within the body. Due to the fact that ultrasound images are collected in real-time, they can also display blood moving through blood arteries and internal organ movement [11].

Endoscopy: A test to examine your internal organs is an endoscopy. An endoscope is a long, thin tube with a tiny camera inside that is inserted into your body through a natural orifice, like the mouth [12].

Elastography: A non-invasive medical imaging technique called elastography can be used to assess the rigidity of organs and other body components. The liver is most frequently evaluated using it.

The liver is subjected to painless, low-frequency vibrations during elastography. The speed at which these vibrations flow through the organ is measured using ultrasound

Figure 1.6: Diabetic Retinopathy

(US) or magnetic resonance imaging (MRI). This data is used by a computer to produce a visual representation of the liver's stiffness (or elasticity) [13].

In addition, we can cite other biomedical imaging techniques like tactile imaging, thermography, single-photon emission computed tomography (SPECT) and medical photography.

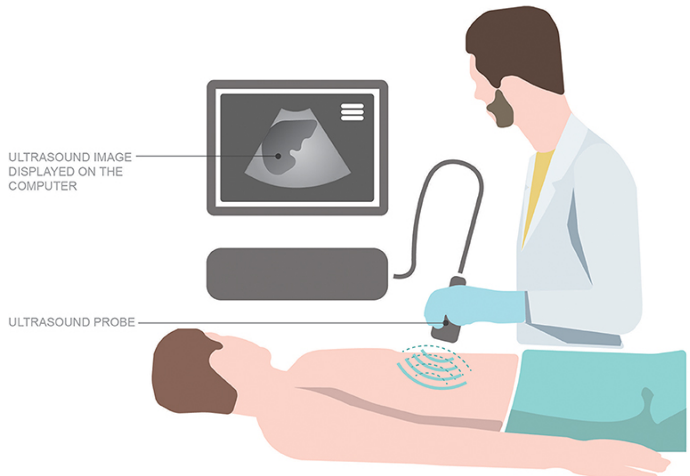

Figure 1.7: Ultrasound

Figure 1.8: Endoscopy

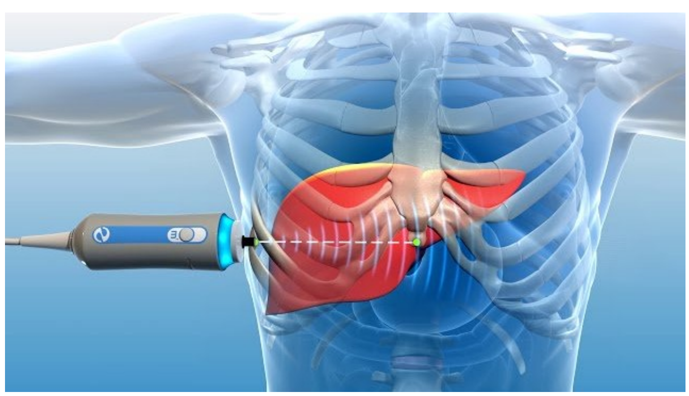

Figure 1.9: Elastography

1.4 ARTIFICIAL INTELLIGENCE

1.4.1 Definition of AI

The definition of AI proposed by Schuett[14] emphasizes that AI systems are designed by humans and operate in both the physical and digital realms. These systems are designed with a complex goal in mind, and their ability to perceive their environment is critical to achieving that goal. To do this, AI systems use data acquisition methods to collect structured and unstructured data, which they then interpret and reason on to derive knowledge and information. Based on this knowledge, they make decisions about the best action(s) to take to achieve the given goal.

It is worth noting that AI systems can use different approaches to achieve their objectives. These approaches may include rule-based methods, where the system follows pre-determined rules to make decisions, logic-based methods, where the system uses reasoning and inference to make decisions, or learning-based methods, where the system learns from examples and data to make decisions. Often, AI systems will use a combination of these approaches to achieve their goals, and the specific approach used will depend on the context and the nature of the problem being solved. Overall, the proposed definition of AI provides a comprehensive understanding of the key characteristics of these systems and the various methods they use to achieve their objectives, as showing in the figure 1.10 [15] below: .

AI can be divided into two types: narrow or weak AI, and general or strong AI. Narrow AI is designed to perform a specific task, while general AI can perform any intellectual task that a human can do, and can reason, learn, and adapt to new situations.

AI has the potential to revolutionize many industries and fields, from healthcare and transportation to finance and education [16].

1.4.2 Historical background

Artificial intelligence (AI) has its roots in the early 20th century, with the concept of ”robotics” first introduced in Karel Capek’s novel R.U.R. in the 1920s. In the 1940s and

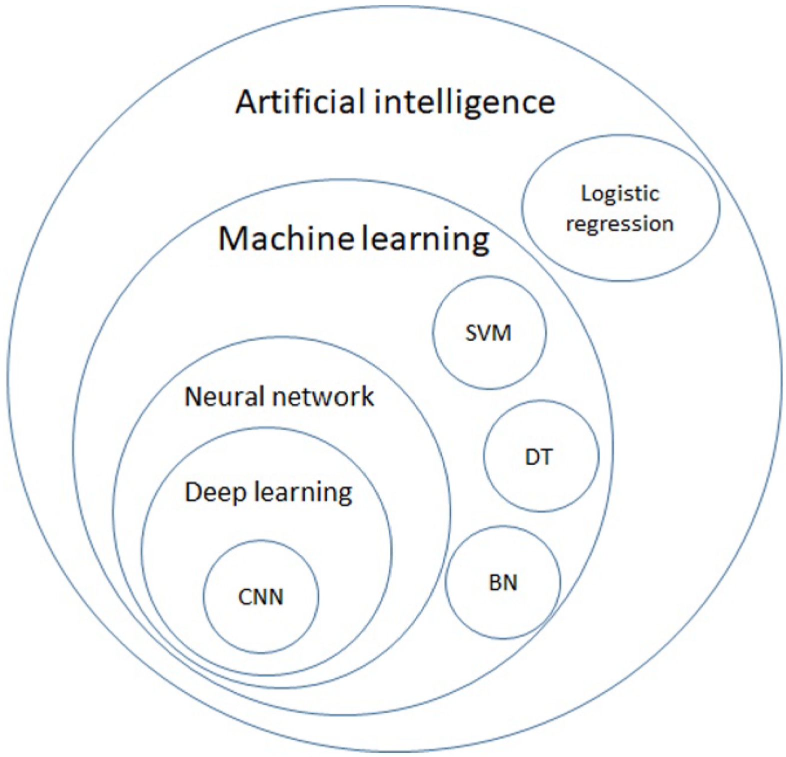

Figure 1.10: Venn diagram of artificial intelligence (AI), machine learning (ML), neural network, deep learning, and further algorithms in each category

1950s, researchers began exploring the mathematical basis for AI, with early work by Alan Turing and others. The term "AI" was first coined by John McCarthy in 1955 and the Dartmouth Conference in 1956 marked the birth of modern AI research.

The history of artificial intelligence (AI) is lengthy and includes various eras. Following are some significant occasions and turning points in AI history [17], listed by era:

- Before 1950: Early computer pioneers like Charles Babbage and Ada Lovelace laid the foundation for the creation of AI.
- The 1950s and 1960s were the "golden age" of AI, which was characterised by the Dartmouth Conference and the earliest developments in computer vision, natural language processing, and machine learning.
- 1970s–1980s: The "AI winter," a time of decreased funding and interest in AI as a result of overly optimistic predictions and a lack of advancement.

- 1970s–1980s: The "AI winter," a time of decreased funding and interest in AI as a result of overly optimistic predictions and a lack of advancement.
- The 1990s and 2000s saw a renaissance in AI thanks to developments in robotics, natural language processing, and machine learning.
- the 2010s and continues today, the development of virtual assistants and self-driving cars, as well as improvements in image recognition, natural language processing, and game play, are all hallmarks of the deep learning revolution, which started in.

Artificial Intelligence in Medicine has evolved AI has the potential to transform healthcare by improving patient outcomes and reducing medical errors through the use of machine learning and deep learning techniques. These techniques enable the analysis of large amounts of medical data, such as electronic health records, medical images, and genomics data, to identify patterns and insights that can help clinicians make more informed decisions. Furthermore, AI can be used to develop predictive models that can identify patients at risk of developing specific diseases or complications, leading to early intervention and preventive measures. However, data quality and privacy concerns need to be addressed before the full integration of AI into medicine can be realized [18].

1.4.3 Machine learning ML

Machine Learning is a subfield of Artificial Intelligence that involves developing algorithms and models that can automatically learn patterns and insights from data without being explicitly programmed. Machine Learning is a powerful tool for solving real-world problems, as it allows organizations to extract valuable information from their data and make data-driven decisions.
The Machine Learning can be divided into three main categories: supervised learning, unsupervised learning, and reinforcement learning table 1.1 .
The Machine Learning has a wide range of applications, including image and speech recognition, natural language processing, fraud detection, and predictive maintenance,

Table 1.1: Machine Learning categories.

Categories	Algorithms
Supervised Learning	Linear Regression, Decision Trees, Random Forest, Support Vector Machines
Unsupervised Learning	K-Means Clustering, Principal Component Analysis, Apriori Algorithm
Reinforcement Learning	Q-Learning, Deep Reinforcement Learning

among others.[18].

1.5 Deep learning DL

Deep Learning is a subfield of machine learning that employs neural networks with multiple layers to learn representations of data with multiple levels of abstraction. It is able to learn from large amounts of data with minimal human intervention and has shown remarkable performance in a variety of applications, including computer vision, natural language processing, and speech recognition [19].

Traditional learning relies on hand-crafted rules and expert knowledge, while Deep Learning learns features directly from data without explicit programming. Deep Learning uses neural networks with multiple layers to learn complex representations from large datasets and generalize to new data as showing in the figure 1.11.

1.5.1 Deep learning techniques

Deep Learning is a subfield of machine learning that involves training neural networks with multiple layers to perform complex tasks, such as image recognition, speech recognition, and natural language processing.

Deep Learning techniques include Convolutional Neural Networks (CNNs) for image processing, Recurrent Neural Networks (RNNs) for sequential data, and Generative Adversarial Networks (GANs) for generating realistic synthetic data. [20].

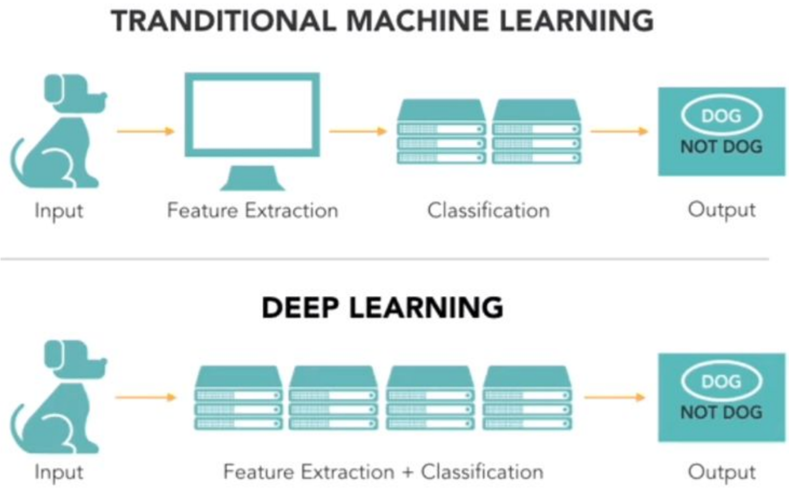

Figure 1.11: Deeplearning and tarnditional learning

Convolutional Neural Networks (CNNs)

Convolutional neural networks (CNNs) are a subclass of deep neural networks that excel in analyzing 2D data, such as photographs. Convolution is a technique used by CNNs, which includes computing the dot products between the input and the filter at each position while sliding a filter (sometimes referred to as a kernel) across the input data (figure 1.12). This process creates a feature map that highlights the input's components that are most crucial to the job at hand. CNNs may learn progressively complicated representations of the input data by stacking numerous convolutional layers, pooling layers, and fully connected layers. As a result, they are able to perform at the cutting edge on a variety of image identification, classification, and segmentation tasks[21].

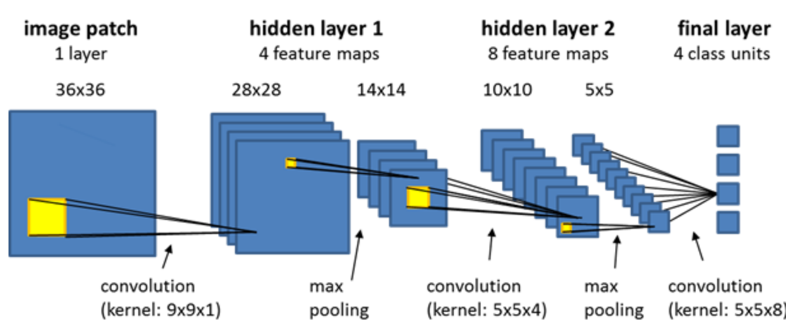

Figure 1.12: Convolutional Neural Networks scheme architecture

Recurrent Neural Networks (RNNs):

Recurrent Neural Networks (RNNs) are a subclass of neural networks that, as shown in figure 1.13, may handle sequential data by keeping an internal state, or "memory," of prior inputs. This enables RNNs to learn and predict patterns in text data, such as natural language phrases, as well as time series data, such as market prices or audio signals. RNNs employ feedback connections to let information to flow from one time step to the next, which enables them to analyze current inputs while taking into consideration the context of earlier inputs. As a result, RNNs are particularly useful for applications like language modeling, speech recognition, and machine translation that call for a comprehension of sequential information. In recent years, there have been significant advances in the design and training of RNNs, including the use of Long Short-Term Memory (LSTM) and Gated Recurrent Unit (GRU) cells, which have greatly improved their performance on a range of applications.

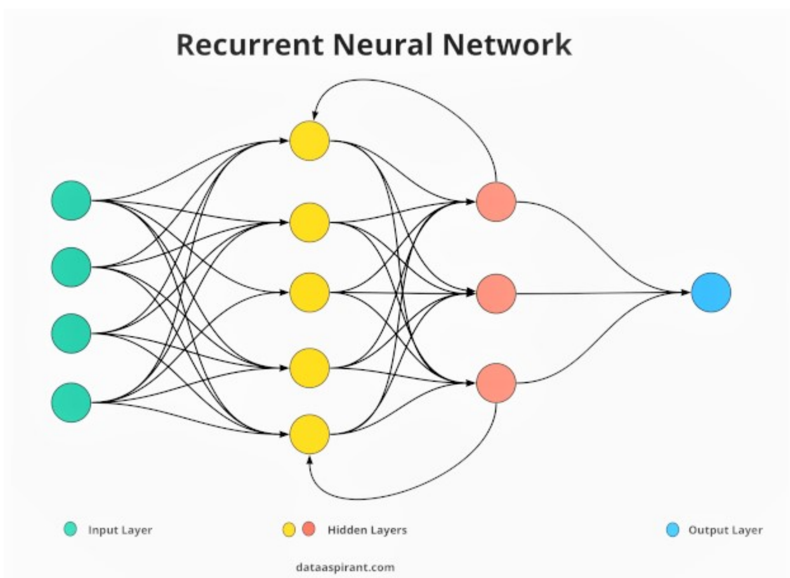

Figure 1.13: Recurrent Neural Network architecture

Transfer Learning

Using information from one task to improve performance on a related activity is a component of the machine learning approach known as transfer learning. In transfer learning, a model trained on a source task can be adjusted for a target task by leveraging the knowledge and representations learned from the source task. When the target task is linked to the source task, as in figure 1.14, or when there are limited data sources for the target work, this strategy can be extremely beneficial.

Several different applications, such as speech recognition, computer vision, and natural language processing, among others, have successfully exploited transfer learning. Transfer learning makes it possible for models to use data from related activities, reducing the amount of data needed for model training and improving model performance. [22].

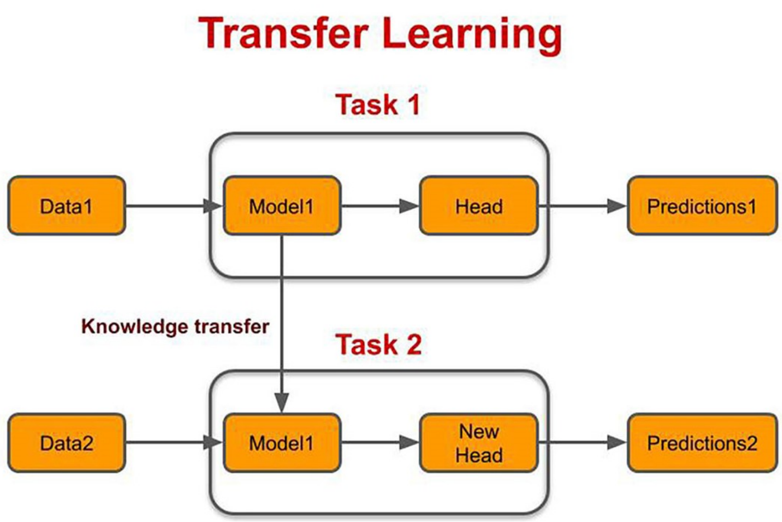

Figure 1.14: Transfer Learning

Generative Adversarial Networks (GANs)

A "generative adversarial network" (GAN) is a deep learning system that combines two opposingly trained neural networks, the discriminator and the generator. In figure 1.15, this training procedure is depicted. The generator learns to create current synthetic data while the discriminator learns to distinguish between real and false data. GANs have been used for a number of tasks, including as style transfer, text-to-image synthesis, and the creation of both still and moving pictures. Yet there are still problems that need to be fixed, such mode collapse and training stability, which has inspired continuing research projects to improve and broaden the capabilities of GANs.

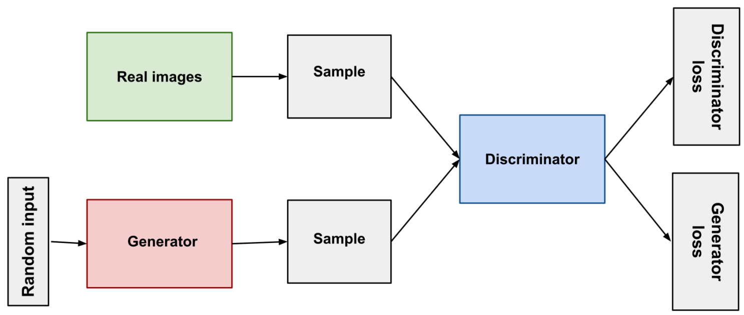

Figure 1.15: Generative Adversarial Networks diagram

Other technique

Autoencoders: Autoencoders are a particular variety of feedforward neural network where input and output are the same. Autoencoders were created by Geoffrey Hinton in the 1980s to address issues with unsupervised learning.

Deep Belief Networks (DBNs): DBNs are generative models made up of a number of layers of latent, stochastic variables. Latent variables, often known as hidden units, have binary values. Each RBM layer in a DBN can communicate with both the layer above it and the layer below. For image, video, and motion-capture data recognition DBNs are employed.

Long Short-Term Memory (LSTM) Networks: LSTMs are a type of Recurrent Neural Network (RNN) that can learn and memorize long-term dependencies. Over time, LSTMs preserve information. Because to their ability to recall prior inputs, they are helpful in time-series prediction. LSTMs are frequently employed for voice recognition, music creation, and drug research in addition to time-series predictions.

Multilayer Perceptrons (MLPs): MLPs are a kind of feedforward neural networks that contain many layers of activation-function-equipped perceptrons. A completely coupled input layer and an output layer make up MLPs. They may be used to create speech recognition, picture recognition, and machine translation software since they have the same number of input and output layers but may have several hidden layers.

Restricted Boltzmann Machines (RBMs): This deep learning algorithm is used for dimensionality reduction, classification, regression, collaborative filtering, feature learning, and topic modeling. RBMs constitute the building blocks of DBNs [23].

Each of these methods has certain advantages and disadvantages, and the best method to use will frequently depend on the particular issue at hand. To overcome the difficulties of practical applications, deep learning researchers and practitioners are continually creating new methods and improving those that already exist.

1.6 Transfer Learning

1.6.1 Transfer Learning Technique

TRANSFER LEARNING in the context of computer vision and deep learning. P(X) is a distribution of values contained in X that produces a set of images. In an image classification problem, Y has all the possible labels, for example cats or dogs. f() is the deep learning model trained to classify an image x into a label y, that can be one of the labels in Y. The training process consists of updating this model based on the domain D, as shown in Figure 1.16 .

This model may be enhanced by transfer learning using the information from a source domain (DS) and a source task (TS). Transfer learning is not relevant when the source and target domains are the same since both the source and the target are attempting to resolve exactly the same problem [24].

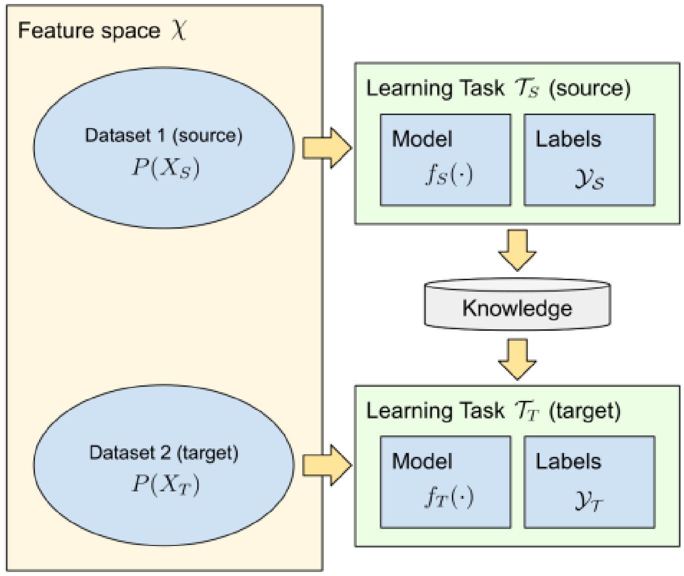

Figure 1.16: Representation of transfer learning [23]

1.6.2 Advantages of Transfer Learning

Transfer learning's primary advantages are resource savings and increased effectiveness while developing new models. Also, since the majority of the model will have already been trained, it can aid with model training when only unlabelled datasets are available.[25]. Here are some of the advantages of transfer learning:

1. **Reduced Training Time:** Transfer learning allows the reuse of pre-trained models and their associated weights, which significantly reduces the amount of training data and computational resources required. This leads to faster training times, allowing for the rapid development and deployment of deep learning models.

2. **Improved Model Performance:** Pre-trained models are often trained on large datasets, and therefore, they have learned rich representations of the input data. By leveraging these pre-trained models, transfer learning can improve the performance of the model on the new task, even when only limited amounts of labeled data are available.

3. **Better Generalization:** Transfer learning enables the model to learn more robust

and generalized features that are transferable across different tasks and datasets. This leads to better generalization capabilities of the model, making it more effective in real-world scenarios.

4. **Requires Less Data:** Transfer learning can be used to train models with less data, making it ideal for scenarios where only limited amounts of labeled data are available.

5. **Cost-Effective:** Transfer learning reduces the cost of training deep learning models by reusing pre-trained models and their associated weights, which significantly reduces the amount of computational resources required.

1.6.3 Framework for Transfer Learning

Microsoft Cognitive Toolkit (CNTK): CNTK is an open-source deep learning framework developed by Microsoft Research. It supports various neural network architectures, including Feedforward, Convolutional, Recurrent, LSTM, and Sequence-to-Sequence networks. Users define networks using a configuration file, and it provides multiple language APIs for CPU or GPU execution. CNTK is designed to be efficient, minimizing computations, memory usage, and system resources.[26].

TensorFlow: TensorFlow is an open-source framework developed by Google Brain for building and executing large computing graphs. It uses a data flow graph to represent numerical operations, allowing for flexibility and experimentation with deep neural network models. TensorFlow is utilized in various industries to put machine learning systems into practice. It supports multiple language APIs, including Python, C++, and Java, making it accessible to developers from different programming backgrounds. [26].

Keras: Python was used to create the open source DL framework. It utilizes the CNTK, Theano, or TensorFlow frameworks as its base. In 2015, Google developer Chollet established Keras as a component of the ONEIROS (Open-ended Neuro-Electronic Intelligent Robot Operating System) research project. Deep neural network rapid expression and simple, quick prototyping are made possible by Keras' design (modularity and extensibility) [26].

PyTorch: PyTorch is a machine learning framework produced by Facebook in October 2016. It is built on the well-liked Torch library and is open source. designed to offer excellent flexibility and quick construction of deep neural networks. As opposed to other deep learning frameworks, PyTorch makes advantage of dynamic computation graphs. In contrast to dynamic graphs, which are generated "on the fly" through forward computing, static computational graphs (such as those used in TensorFlow) are specified before execution. In other words, every iteration involves starting again with the graph. [27].

There are several popular frameworks available for implementing transfer learning, each with its own advantages and disadvantages. this is most popular frameworks for transfer learning that provide rich APIs and tools for building and training machine learning models.

1.6.4 Transfer Learning Models

Machine learning models may now be trained effectively via transfer learning. We can enhance a model's performance on a separate but related task or domain by applying what model learn from one task or domain. Many transfer learning models have been put out recently and have produced cutting-edge outcomes on a variety of tasks. this some of the popular transfer learning models:

For computer vision:

VGG Family: The network is distinguished by its simplicity, consisting merely of a stack of three 3x3 convolutional layers on top of each other, with the max-pooling layers handling the growing depth and volume size. Then comes a softmax layer, which is followed by two fully linked layers with 4096 nodes each. [28].

ResNet: ResNet is a type of unusual architecture that depends on microarchitecture modules, which the architecture refers to as a network. The set of components known as microarchitecture is what is utilized to create a brand-new network. First introduced by

Kaiming He in 2015 [29].

For NLP tasks:

BERT: In 2018, Google created the pre-trained NLP model known as Bidirectional Encoder Representations from Transformers BERT. It uses a transformer-based architecture to train a model that is capable of completing a variety of tasks at a SOTA level. In 11 NLP tasks, including the Stanford competitive QA dataset, Google demonstrated its capabilities [30].

GPT-3: Pre-trained NLP models were produced by OpenAI. A 10x larger model than earlier ones, GPT-3 is a large-scale transformer-based language model that was trained on 175 billion parameters. The business has demonstrated its exceptional abilities for projects including translation, Q&A, and word unscrambling. This third-generation language prediction model is autoregressive in nature and functions similarly to conventional models in that it receives input vectors of words and makes predictions about the results based on its training [30].

Transfer learning models have become popular in recent years due to their effectiveness and efficiency. These models have achieved state-of-the-art results on various benchmarks and are widely used in academia and industry.

1.6.5 Transfer Learning Optimization

Increasing the efficacy and efficiency of transfer learning models is the aim of transfer learning optimization. Optimization is a key component of deep learning, which involves training complex neural network models on large datasets. It entails employing gradient-based optimization methods, such as SGD and its variations, to iteratively update model parameters. Optimization faces various difficulties, including scalability, convergence, and overfitting. In order to overcome these difficulties, researchers have created a variety of methodologies, including more sophisticated optimization algorithms, regularization techniques, and adaptive learning rate methods [31].

Chapter 2

DEEP TRANSFER LEARNING FOR DISEASE ANALYSIS

2.1 Introduction

Modern medicine relies heavily on disease classification since it helps with diagnosis, treatment planning, and overall healthcare quality.

By examining data from photos of these diseases and diagnostics, models may be trained to identify the particular patterns and signs of these diseases using in-depth learning techniques. We will use this method to identify a variety of diseases, including those affecting the brain, Alzheimer's disease, the stomach, the chest, and the skin.

2.2 State of the Art

2.2.1 Brain tumor

Definition: A brain tumor is a growth of cells in the brain or near it. And can also happen near the brain tissue. Nearby locations include nerves, the pituitary gland, the pineal gland, and the membranes that cover the surface of the brain. Noncancerous brain tumors may grow over time, while malignant brain tumors can quickly invade and destroy the brain tissue.

Brain tumors range in size from very small to very large (Fig.2.1). Some are found when they are small, while others grow large before they are detected. Some parts of the brain are less active, so a brain tumor may not cause symptoms right away [32].

Related Work: Some related work on the Brain Tumor from these papers [33] and '[34] is shown in Table 2.1.

Table 2.1: Summary of Brain Tumor Segmentation Results

Paper	**Year**	**Dataset**	**Technique and Model**	**Accuracy**
Irmak et al. [35]	2021	MRIs	Deep Convolution with Fully Optimized Framework (DC-FOF), CNN	98.14%
Munir et al. [36]	2021	BraTS 2019 dataset	2D-UNET CNN	Dice coefficient: 0.9694
Biratu et al. [37]	2021	BraTS2015 dataset	Enhanced region-growing approach, Thresholding, Deep learning	90%
Chahal et al. [38]	2021	MRIs (DICOM dataset)	Hybrid weighted fuzzy approach, Fuzzy clustering, SVM	97%
Maqsood et al. [39]	2022	Brain tumors	Linear contrast stretching, Neural network architecture, MobileNetV2 architecture, Multiclass SVM (M-SVM)	Accuracy: 97.47% (BraTS 2018 dataset), 98.92% (Figshare dataset)
Rajinikanth et al. [40]	2022	Brain tumors (TCIA dataset)	Pre-trained VGG16 and VGG19, Pooling methods, SoftMax	>99%
Badjie and Ülker [41]	2022	Brain MRI	AlexNet's convolutional neural network (CNN)	99.62%
Alanazi et al. [42]	2022	3000 MRI images (from Kaggle)	CNN	96.89%
Zahid et al. [43]	2022	MRI images (native, post-contrast, T2, T2 FLAIR)	ResNet101	94.4%

Figure 2.1: Brain tumor

2.2.2 Alzheimer's disease

Definition: Alzheimer's disease is a term for memory loss and other cognitive impairments severe enough to interfere with everyday living. 60-80% of cases of dementia are caused by Alzheimer's disease, which is not a typical aspect of aging. Younger-onset Alzheimer's disease is another name for younger-onset dementia and can be in the early, medium, or late stages (Fig 2.2). Aging is the biggest risk factor now understood[44].

Figure 2.2: Progression alzheimers disease

Related Work: Summary of some related papers' works in Alzheimer's disease classification and detection in the table 2.2.

Table 2.2: Summary of papers on AD classification

Paper	Year	Dataset	Model	Accuracy
C. V. Angkoso, et al.[45]	2022	1500 MRI Data from ADNI dataset	Mp-CNN	93%
L. Heising, S. Angelopoulos [46]	2022	3312 MRI images	LENet-5	84%
M. W. Oktavian, et al. [47]	2022	MRI and PET data	Finetuned ResNet18	88.3%
E. Yee, et al. [48]	2021	ADNI data (sDAT and sNC)	3D CNN with dilated convolutions	88%
M. Odusami, et al. [48]	2022	MRI images	ResNet18, DenseNet201	98.89%
M. Odusami, et al. [49]	2021	MRI data from ADNI	ResD hybrid model (ResNet18, DenseNet121)	N/A
M. Odusami, et al. [50]	2021	OASIS database's MRI images	Pre-trained models (SqueezeNet, ResNet18, AlexNet, VGG16, DenseNet, InceptionV3)	82.53% (SqueezeNet)
N. Deepa, S. P. Chokkalingam [51]	2022	T1-weighted MRI images (pre-processed with CAT12 toolbox)	Optimized VGG-16 (AOA)	97.89%
P. Pandey, A. Khare, P. Srivastava [52]	2022	MRI brain images (ADNI dataset)	CNN models (GoogLeNet, ResNet50, AlexNet, ResNet18, DenseNet, SqueezeNet)	96.81% (GoogLeNet)
A. Bhagat, et al. [53]	2023	MRI datasets	MobileNet (transfer learning)	96.6%
X. Xing, et al. [54]	2023	3D PET brain images	Learnable Weighted Pooling + 2D model (ResNet34)	88%

2.2.3 Respiratory disease

Definition: A condition that affects the respiratory system's lungs and other organs. Infections, cigarette use, exposure to secondhand smoke, radon, asbestos, and other types of air pollution can all lead to pulmonary disorders. Asthma, chronic obstructive pulmonary disease (COPD), tuberculosis (TB) (Fig 2.3), pneumonia, COVID-19, and lung cancer are examples of Lung diseases[55].

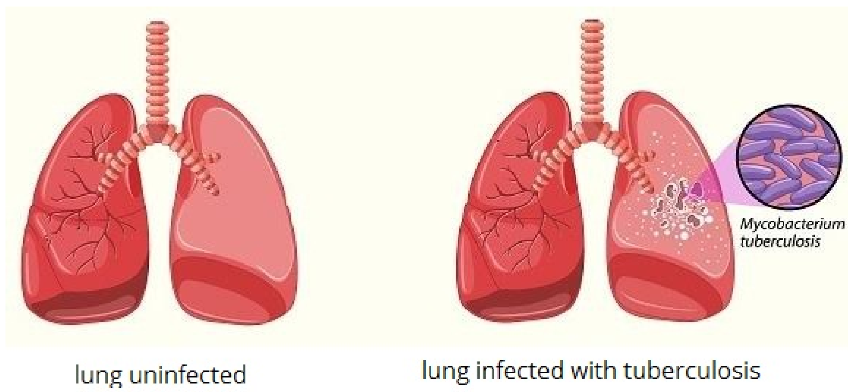

Figure 2.3: Lungs, both healthy and tuberculous

Related Work: Summary of some related papers' works in Respiratory diseases detection and classification in Table 2.3.

Table 2.3: Some of Respiratory Disease Detection Methods

Reference	**Year**	**Model**	**Data**	**Accuracy per-task (%)**
Ucar et al. [56]	2020	Deep-SqueezeNet	76 COVID-19, 4,290 Non-COVID-19 pneumonia, 1,583 Normal	98.30 (Three groups)
Waheed et al. [57]	2020	COVIDGAN	403 COVID-19, 721 Normal	95.00 (Two groups)
Chen et al. [58]	2020	2D Unet++	51 COVID-19, 55 Other disease	92.59
Gunraj et al. [59]	2020	2D CNN	-	99.10
Wang et al. [60]	2020	3D Unet + 3D TCNN	1,315 COVID-19, 2,406 ILD, 936 Normal	93.30
Song et al. [61]	2021	Shared 2D CNNs	88 COVID-19, 100 Bacterial pneumonia, 86 Normal	93.00
Acar et al. [62]	2021	BDCUnet + GAN + 2D CNN	1,607 COVID-19, 1,667 Normal	99.51
Hu et al. [63]	2020	2D Unet + 2D WS-CNN	80 COVID-19, 78 Pneumonia, 72 Normal	87.4
Wang et al. [64]	2020	2D Unet + 3D WS-CNN	313 COVID-19, 299 Non-COVID-19	90.10

2.2.4 Skin cancer

Definition: Skin cancer is a condition marked by the uncontrolled proliferation of skin cells. Nonmelanoma and melanoma are two different forms of skin cancer. Together, they represent around 50% of all cancers that have been recorded. The most prevalent malignancies in the United States are nonmelanomas, which are much less hazardous than melanomas, which are tumors of pigmented cells [65].

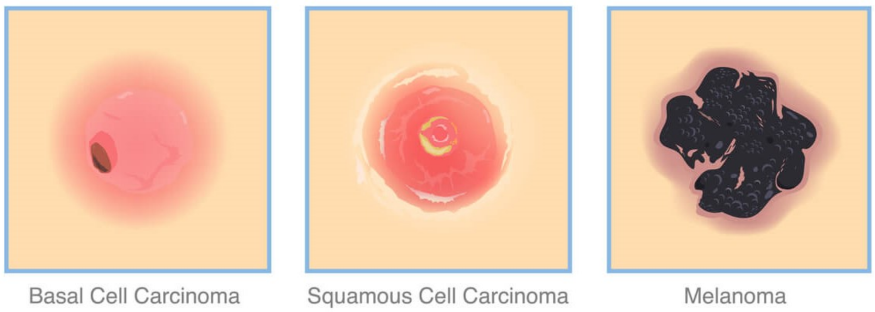

Figure 2.4: Type of Skin cancer

Related Work: Summary of some related papers' works in Skin cancer classification in the table 2.4.

Table 2.4: Summary of Segmentation Approaches for Skin

Paper	**Year**	**Methods**	**Datasets**	**Results**
Abdulhamid et al. [?]	2020	Median filter, histogram, Auxiliary function, global optimization algorithm	PH2, ISBI 2016, ISBI 2017	ACC: 0.932, 0.952, 0.976
Saravanan et al. [66]	2020	Median filter, contrast stretching, ABCD, Threshold-based segmentation	DermIS, DermQuest	ACC: 1.00
Hawas et al. [67]	2020	GA, OCE-NGC	ISIC 2016	ACC: 0.976
Öztürk et al. [68]	2020	Ifcn	PH2, ISBI 2017	ACC: 0.969, 0.953
Huang et al. [69]	2020	LabelMe, R-CNN	ISIC	Recall: 0.910
Shan et al. [70]	2020	Augmentation, resizing, FC-DPN	ISBI 2017, PH2	JAC: 0.800, 0.835
Ashour et al. [71]	2021	Dull razor, Initial contour optimization, GA	ISIC 2016	JAC: 0.831
Kaur et al. [72]	2022	Downsampling, translation, rotation and scaling, Atrous dilation CNN	ISIC 2016, 17, 18	JAC: 0.904, 0.818, 0.891
Mohakud et al. [73]	2022	Image Resize, FCEDN, EN-GWO	ISIC 2016, 17	JAC: 0.964, 0.868

2.2.5 Gastrointestinal Disease

Definition: A gastrointestinal disease is one that affects the GI tract, which is the passageway connecting the mouth and the anus, or stomach. Irritable bowel syndrome (IBS), acid reflux, indigestion, colon cancer (Fig.2.5), and hemorrhoids are a few common GI conditions. In order for the body to absorb and use nutrients to maintain health, digestion takes place in the GI tract. Numerous GI conditions impair your body's typical capacity to digest food.

These include In contrast to structural GI disorders, which originate when there is a change or issue with the GI tract's structural integrity, functional GI diseases are defined by chronic (long-term) GI symptoms that result from the function or dysfunction of the digestive system. The GI tract can contain these structural problems anywhere[74].

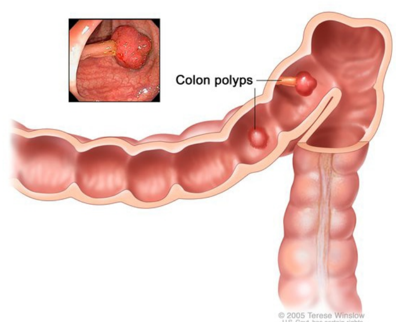

Figure 2.5: colon cancer

Related Work: A summary of some related papers' works in gastrointestinal disease detection and classification is shown in Table 2.5.

Table 2.5: Summary of Gastrointestinal Tract Disease Classification Methods

Paper	**Year**	**Methods**	**Datasets**	**Results**
Yogapriya et al. [75]	2021	KvasirV2 dataset	VGG16, ResNet-18, GoogLeNet	96.33% (VGG16)
Öztürk and Özkaya [76]	2021	LSTM-based classifier (AlexNet, GoogleNet, ResNet)	KvasirV2 dataset	97.90%
Öztürk and Özkaya [77]	2021	Residual LSTM layer CNN	KvasirV2 dataset	98.05%
Dutta et al. [78]	2022	Tiny Darknet model	HyperKvasir dataset	75.80% (MCC)
Ramamurthy et al. [79]	2022	Multi-feature fusion (Efficient-NetB0, Effimix)	HyperKvasir dataset	97.99%
Khan et al. [80]	2022	Transfer learning (MobileNet-V2)	KvasirV2 dataset	98.02%
Khan et al. [81]	2022	Moth-crow optimization with DCCA fusion	HyperKvasir dataset	97.20%
Mohapatra et al. [82]	2022	Empirical wavelet transform (EWT) and CNN	HyperKvasir dataset	96.65% (stage 1), 94.25% (stage 2)
Afriyie et al. [83]	2022	Denoising capsule networks (Dn-CapsNets)	KvasirV2 dataset (5 classes)	94.16%
Wang et al. [84]	2022	CNN and capsule networks	KvasirV2, Hyper-Kvasir dataset	94.83% (KvasirV2), 85.99% (Hyper-Kvasir)

2.3 Deep Transfer Learning Models

In this project, we will use three strong deep learning models: ResNet50, EfficientNet-B3, and DenseNet121. These models have become quite popular and have shown astounding performance in a variety of computer vision applications, including medical picture analysis.

2.3.1 ResNet50

ResNet50 is not the first model to come from the ResNet family. The original model was called the Residual Net, or ResNet, This network consists of 64 kernels, a stride 2 by 3 by 3 max pooling layer, a stride 7 avg pooling layer, 16 residual construction blocks, and a fully linked layer at the bottom. There are around 23 million trainable parameters in this network. Fig. 2.6 presents ResNet50's architectural layout [85].

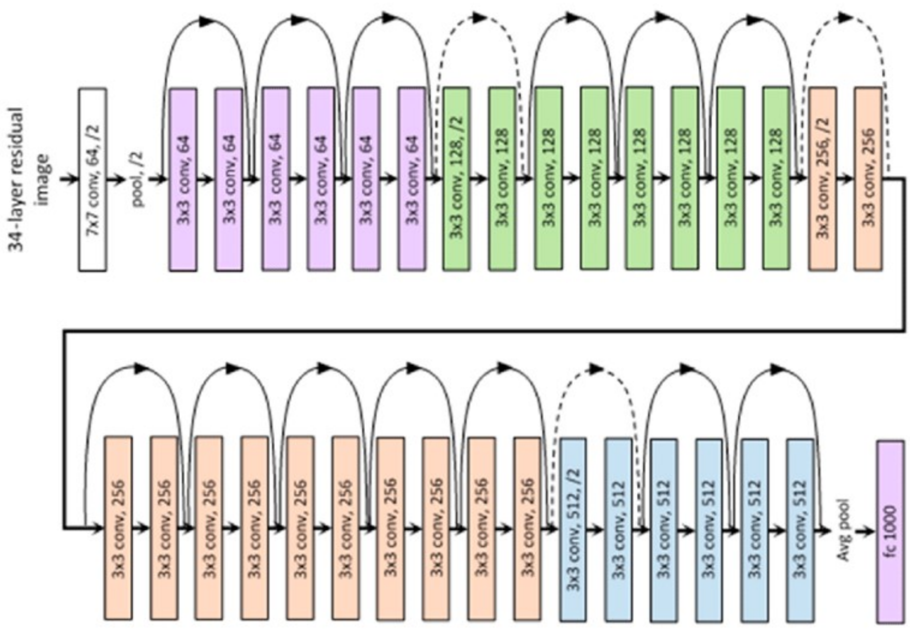

Figure 2.6: Architecture of ResNet-50 pre-trained deep learning model

2.3.2 DenseNet-121

DenseNet-121 is a deep convolutional neural network (CNN) architecture that exhibits an impressive structure composed of several types of layers. It consists of a 7x7 convolutional layer, followed by 58 3x3 convolutional layers, 61 1x1 convolutional layers, 4 average pooling layers, and finally a fully connected layer, DenseNet-121's architectural layout is shown in Fig. 2.7 [86].

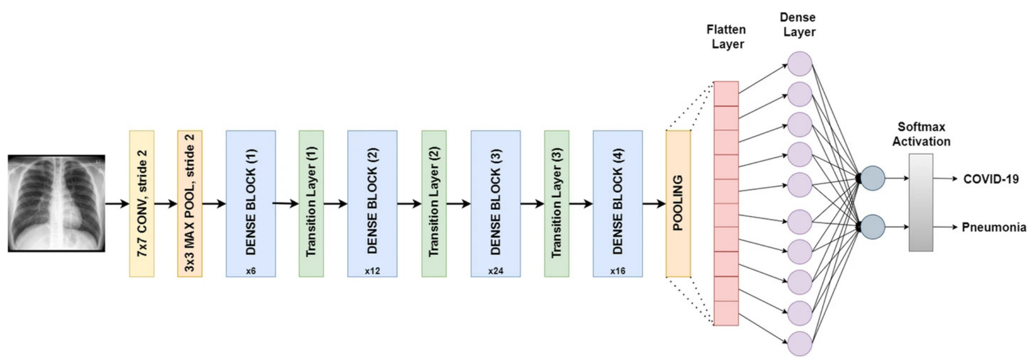

Figure 2.7: DenseNet-121's architectural layout

2.3.3 EfficientNet-B3

EfficientNet is a convolutional neural network design and scaling technique that uses a compound coefficient to consistently scale all depth, breadth, and resolution parameters. The architecture for network EfficientNet-B0 is shown in Fig. 2.8. EfficientNet scaling approach evenly scales network breadth, depth, and resolution using a set of preset scaling coefficients, in contrast to standard practice, which scales these variables arbitrarily [87].

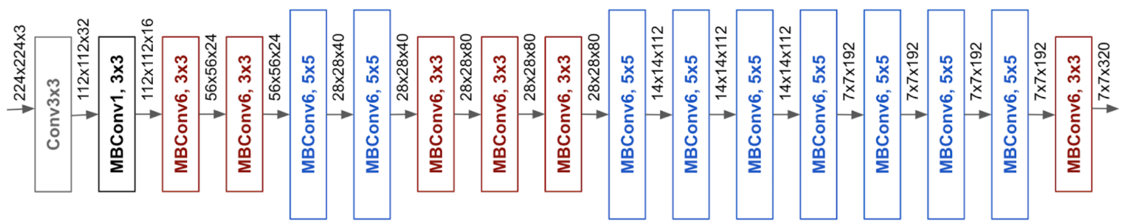

Figure 2.8: The architecture for baseline network EfficientNet-B0

2.4 Data Augmentation

Deep learning applications in particular are expanding and developing at an astounding rate in the machine learning application environment. Data-centric model-building techniques have proven beneficial in overcoming the difficulties faced in the field of artificial intelligence. Techniques for data augmentation have become a potent tool among these methods.

Data augmentation refers to a group of methods intended to increase the amount of data by creating new data points based on current ones, as shown in Fig. 2.9. These methods either use deep learning models to generate new data instances or introduce small changes to the data. Data augmentation helps machine learning models perform better and produce better results by enhancing the dataset. A robust and extensive dataset gives the model more accuracy and effectiveness.

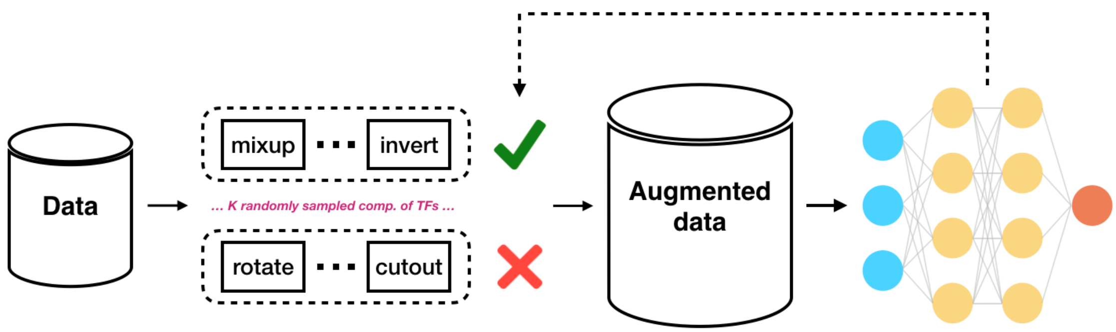

Figure 2.9: A deterministic series of adjusted transformation functions is used in heuristic data augmentations.

The importance of data augmentation lies in its ability to encourage more resilient machine learning models. Data augmentation allows models to be effectively used in a variety of settings by producing versions that replicate real-world events. The resilience of machine learning models is improved by their capacity to extrapolate beyond the boundaries of the initial dataset [88].

2.5 Conclusion

In this chapter, we investigate the application of deep transfer learning in disease analysis and provide insights into the state-of-the-art in different disease domains. Brain tumor analysis, detection of Alzheimer's disease, classification of skin cancer, identification of polyps and detection of respiratory diseases have been studied as prominent examples. Additionally, this chapter examines deep transfer learning models including ResNet50, DenseNet-121, and EfficientNet-B3, which perform well on disease analysis tasks. Data augmentation has been highlighted as a key technique to improve the effectiveness of deep transfer learning models. Artificially augmenting datasets with techniques such as image classification and segmentation and natural language processing (NLP), data augmentation can better generalize models and address different scenarios encountered when analyzing real-world diseases.

Chapter 3

RESULT AND DISCUSSIONS

3.1 Introduction

In this chapter, we evaluate and discuss a number of different experiments carried out using three transfer learning models (ResNet50, DenseNet-121, and EfficientNetB3) on a different dataset on Kaggle that presents a different disease, the Brain Tumor MRI Dataset, Alzheimer MRI Preprocessed Dataset, Chest X-Ray (Pneumonia, COVID-19, Tuberculosis), Skin Cancer, and Gastrointestinal Disease Dataset. Additionally, the data augmentation task is used to improve the system's accuracy. The outcomes are presented as accuracy, recall, accuracy, and f1 score.

3.2 Experimental Protocol

3.2.1 Data Description

Brain Tumor MRI Dataset

This dataset contains 7023 images of human brain MRI images, which are classified into 4 classes: glioma - meningioma - no tumor and pituitary (table. 3.1).

- No tumor class images were taken from the Br35H dataset.

- The glioma class images are used on the figshare site (Fig. 3.1).

This data was uploaded by MASOUD NICKPARVAR [89]

Table 3.1: Number of images in each class for the Brain dataset

Class	# Images
Glioma	1621
Meningioma	1645
No tumor	2000
Pituitary	1757
Total	7023

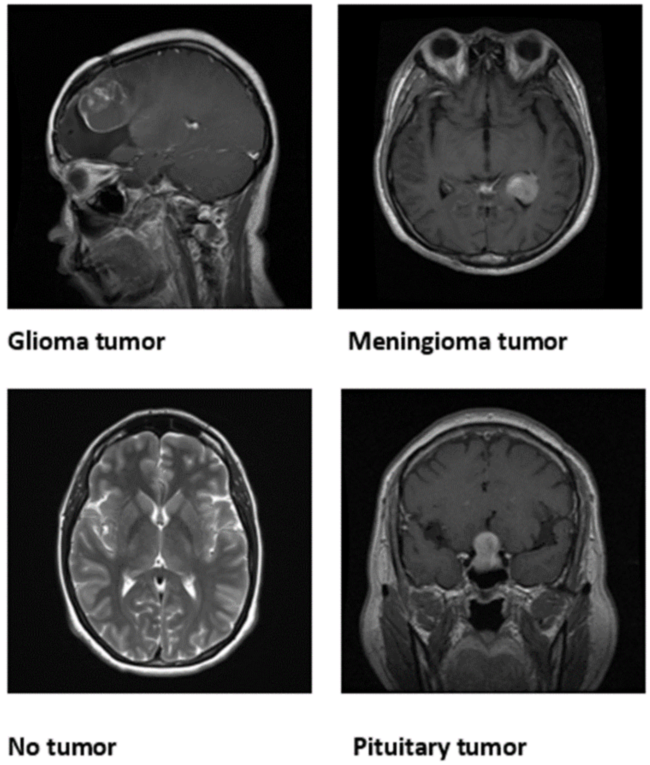

Figure 3.1: Samples belong to the dataset one from each class

Alzheimer MRI Preprocessed Dataset

The preprocessed dataset contains a collection of MRI (Magnetic Resonance Imaging) images for Alzheimer's disease. These images have been gathered from various sources, including websites, hospitals, and public repositories. Each MRI image has been resized to a resolution of 128 by 128 pixels. Samples belong to the dataset shown in Fig. 3.2. The dataset is divided into four distinct classes and comprises a total of 6400 MRI images (Table 3.2).

This data was uploaded by SACHIN KUMAR [90]

Table 3.2: Number of images in each class for the Alzheimer dataset

Class	Image number
Mild Demented	896
Moderate Demented	64
Non Demented	3200
Very Mild Demented	2240
Total	6400

Chest X-Ray (Pneumonia, Covid-19,Tuberculosis)

The dataset is structured in a hierarchical manner with three main folders: train, test, and val. Within each of these folders, there are subfolders representing different categories of images, namely normal, pneumonia, COVID-19, and tuberculosi, Samples belong to the dataset shown in Fig. 3.3. The dataset consists of a total of 7135 x-ray images across all categories (Table 3.3).

This data was uploaded BY JTIPTJ [91]

Table 3.3: Number of images in each class for the Chest X-Ray dataset

Class	Numbers
Covid-19	576
Normal	1583
Pneumonia	4273
Tuberculosis	703
Total	7135

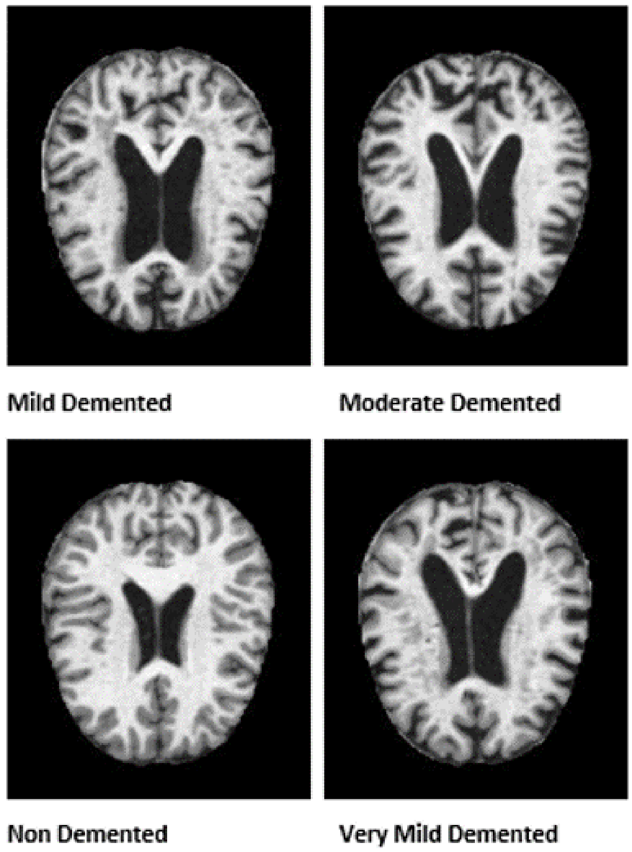

Figure 3.2: Samples belong to the Alzheimer dataset from each class

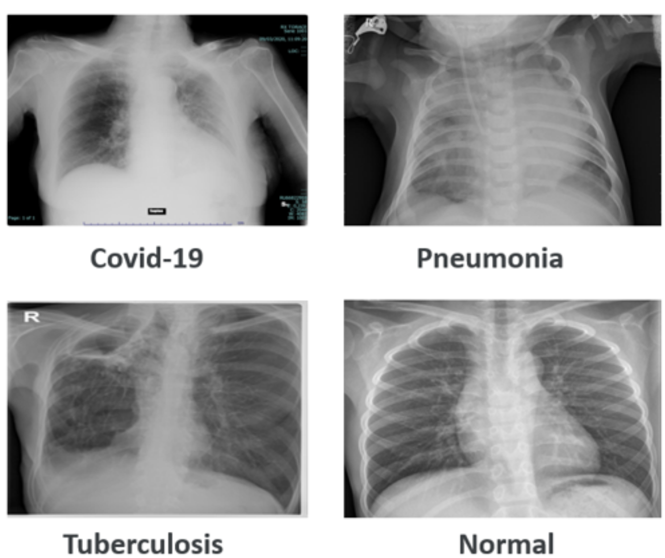

Figure 3.3: Samples belong to the Chest X-Ray dataset from each class

Skin Cancer: Malignant vs. Benign

The dataset provided focuses on skin cancer classification, specifically distinguishing between malignant and benign skin moles, as shown in in Fig. 3.4. It contains a balanced collection of images, with two folders dedicated to each type of mole (Table 3.4), and the images are of size 224x244 pixels.

This data was uploaded by CLAUDIO FANCONI [92]

Table 3.4: Number of images in each class for the Skin Cancer dataset

Class	image Number
Benign	1800
Malignant	1497
Total	3297

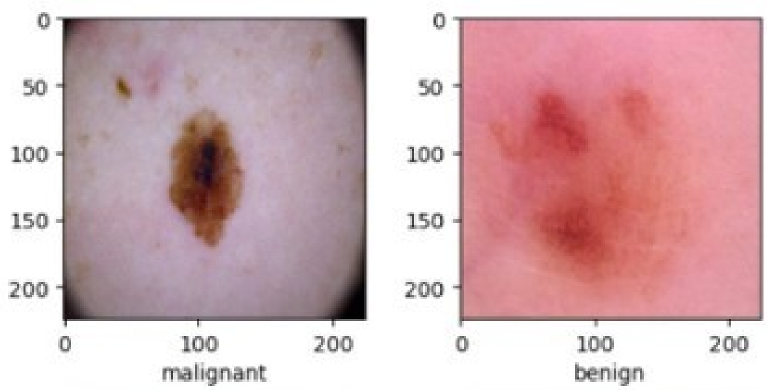

Figure 3.4: Samples belong to the Skin Cancer dataset from each class

Kvasir Dataset

Kvasir is a significant dataset that addresses the scarcity of medical image datasets for computer-aided disease detection. It focuses on gastrointestinal (GI) tract images, classifying them based on three anatomical landmarks and three clinically relevant findings. The dataset also includes two categories of images related to endoscopic polyp removal (Fig 3.5). Medical doctors with expertise in endoscopy have carefully sorted and annotated the dataset. Kvasir is invaluable for researchers exploring single- and multi-disease computer-aided detection, Summary the contain of the data in the table 3.5.

This data was uploaded by MEET NAGADIA [93]

Table 3.5: Number of images in each class for the Kvasir dataset

Class	Image Numbers
dyed-lifted-polyps	500
dyed-resection-margin	500
esophagitis	500
normal-cecum	500
normal-pylorus	500
normal-z-line	500
polyps	500
ulcerative-colitis	500
Total	4000

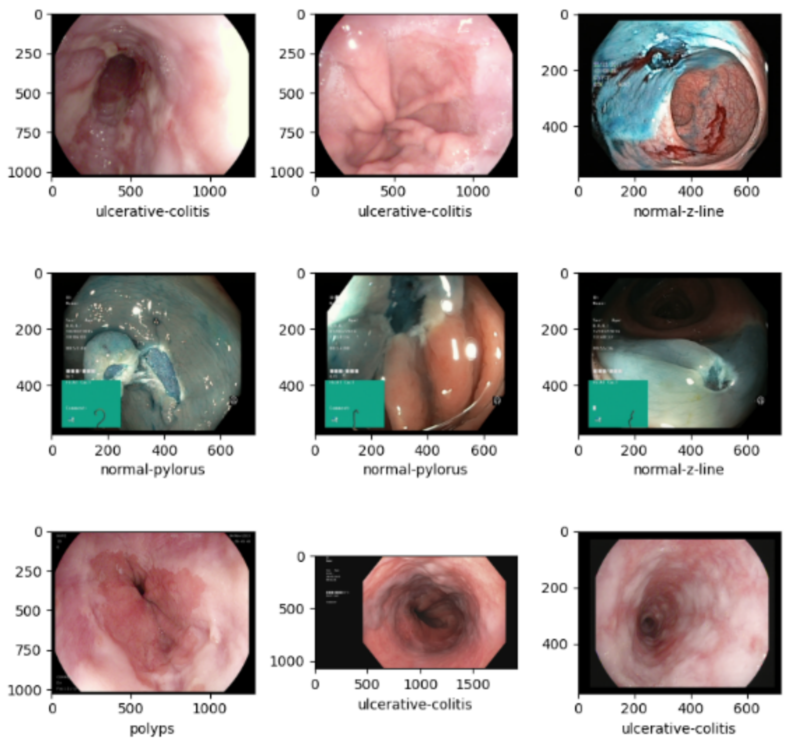

Figure 3.5: Samples belong to the Kvasir dataset from each class

3.2.2 Evaluation Metrics

Evaluation, specifically quantitative evaluation, can serve a variety of functions. The amount of data utilized for training and evaluation may also be subject to a variety of restrictions. Good precision is sometimes prioritized over good recall, and vice versa in other situations.

A development set is utilized when creating a system, and it contains data used to create training rules for a machine learning system.

The development set, also known as the training set in machine learning, is used to teach the system. The machine learning algorithm's errors can be analyzed using a portion of the training set, and the algorithm's parameters can be tuned in response. Development Test Set" is the name given to this portion of the training set.

A test set is put aside to test the artefact, which is not used for development or training. If data is scarce, a method called k-fold cross validation is used to divide the dataset into k folds, with the k-1 folds used for training and the remaining k-1 folds for evaluation. The average is then calculated. Usually 10-fold cross-validation is used [94].

Table 3.6: Confusion matrix: predicted annotation is what the algorithm retrieves or annotates and gold annotation is what was marked up or annotated by a human

		Predicted annotation	
		Positive	Negative
Gold Annotation	Positive	True positive (tp)	False negative (fn)
	Negative	False positive (fp)	True negative (tn)

Two metrics used for measuring the performance of a retrieval system areprecision and recall.Precision measures the number of correct instances retrieveddivided by all retrieved instances, see Formula 3.1.Recall measures the numberof correct instances retrieved divided by all correct instances, see Formula 3.2.Instances can be entities in a text, or a whole document in a document collection(corpus), that were retrieved. A confusion matrix, see Table 3.6 is often used for explaining the different entities [95]. Here follow the definitions of precision and recall, see Formulas 3.1 and 6.2 respectively.

$$\text{Precision: P} = \frac{\text{tp}}{\text{tp +fp}} \tag{3.1}$$

$$\text{Recall: R} = \frac{\text{tp}}{\text{tp +fn}} \tag{3.2}$$

The F-score is defined as the weighted average of both precision and recall depending on the weight function $\beta, seeFormula3.3.TheF1 - scoremeanstheharmonicmeanbetweenprecisionandrecall, seeFormula6.4, whenitiswrittenF - scoreitusuallymeansF1 - score.TheF1 - scorecanhavedifferentindicesgivingdifferentweightstoprecisionandrecall.$

$$F - score : F_\beta = \frac{(1+\beta^2)\cdot P \cdot R}{(\beta^2 \cdot P) + R} \tag{3.3}$$

With $\beta\bar{1}thestandardF - scoreisobtained, seeFormula3.4.$

$$F - score : F_1 = 2 * \frac{P * R}{P + R} \tag{3.4}$$

For the calculation, Precision makes use of every document retrieved. If there are several documents, it may be possible to use precision at a cut-off value to simplify the calculation.

Another metric called accuracy is the percentage of true examples—both positive and negative—among all instances that are retrieved. Precision and inverse precision are weighted arithmetic measures that represent accuracy. A system may function effectively but with high accuracy but low precision; contrast this with striking the bullseye, which entails both high accuracy and high precision. For more information, see Formula 3.5.

$$Accuracy : A = \frac{tp + tn}{tp + tn + fp + fn} \quad (3.5)$$

Abaseline is usually a value for what a basic system would perform. The baselinesystem can be a system working in a random way or be a naïve system. The base line can also be very smart and strong, but the importance of the baseline is to have something to compare with.

If there are other systems using the same data, then it is easy to compare results with these systems and a baseline is not so important[95].

3.3 Testing Experiences

3.3.1 Parameters

In order to obtain good results, we tested our three models on the five datasets. In the first part of the test, we resize all the image in the datasets and used different parameters such as learning rate, type of optimizer, number of epochs, and the values of the batch size to determine which was best for each dataset we had, and this method is important for the next part.

Brain Tumor MRI

The data were divided according to Table 3.7, and the results represented in Table 3.8 were obtained:

Table 3.7: Brain MRI dataset Split

Label Names	**Train Count**	**Validation Count**	**Test Count**
glioma	1296	162	163
meningioma	1316	164	165
notumor	1600	200	200
pituitary	1405	175	177
Total Image Count	**5617**	**701**	**705**

Table 3.8: The results for Brain MRI dataset

MODEL	EPOCH	BATCH SIZE	LAR RATE	OPTEM	TEST ACC
ResNet50	15	8	0.001	SGD	99.01
				ADAM	84.26
				RMSprop	87.65
			0.01	SGD	92.05
			0.0001		97.73
		32	0.001		98.58
		16			99.29
	30	16			99.007
DenseNet-121	15	8	0.001	SGD	99.43
				ADAM	91.48
				RMSprop	96.31
			0.01	SGD	85.67
			0.0001		93.04
		16	0.001		98.72
		32			98.29
	30	16			98.72
EfficientNetB3	15	8	0.001	SGD	98.43
				ADAM	94.61
				RMSprop	95.31
			0.01	SGD	98.44
			0.0001		91.63
		16	0.001		98.29
		32			98.44
	30	32			98.58

Alzheimer MRI

The data were divided according to Table 3.9, and the results represented in Table 3.10 were obtained:

Table 3.9: Alzheimer MRI dataset Split

Label Names	**Train Count**	**Validation Count**	**Test Count**
Mild_Demented	716	89	91
Moderate_Demented	51	6	7
Non_Demented	2560	320	320
Very_Mild_Demented	1792	224	224
Total Image Count	**5119**	**639**	**642**

Table 3.10: The results for Alzheimer MRI dataset

MODEL	EPOCH	BATCH SIZE	LAR RATE	OPTEM	TEST ACC
ResNet50	15	8	0.001	SGD	99.22
				ADAM	55.91
				RMSprop	59.50
			0.01	SGD	56.54
			0.0001		94.39
		16	0.001		99.53
		32			97.99
	30	16			99.06
DenseNet-121	15	8	0.001	SGD	98.44
				ADAM	61.37
				RMSprop	56.23
			0.01	SGD	55.76
			0.0001		71.49
		16	0.001		98.59
		32			93.14
	30	16			98.59
EfficientNetB3	15	8	0.001	SGD	99.22
				ADAM	56.85
				RMSprop	58.25
			0.01	SGD	53.73
			0.0001		97.35
		16	0.001		98.90
		32			97.20
	30	8			99.22

Chest X-Ray

The data were divided according to Table 3.11, and the results represented in Table 3.12 were obtained:

Table 3.11: Chest X-Ray dataset Split

Label Names	**Train Count**	**Validation Count**	**Test Count**
COVID19	460	10	106
NORMAL	1341	8	234
PNEUMONIA	3875	8	390
TUBERCULOSIS	650	12	41
Total Image Count	**6326**	**38**	**771**

Table 3.12: The results for Chest X-Ray dataset

MODEL	EPOCH	BATCH SIZE	LAR RATE	OPTEM	TEST ACC
ResNet50	15	8	0.001	SGD	89.62
				ADAM	71.20
				RMSprop	70.16
			0.01	SGD	80.82
			0.0001		87.67
		16	0.001		88.32
		32			89.49
	30	8			92.00
DenseNet-121	15	8	0.001	SGD	87.67
				ADAM	83.65
				RMSprop	82.61
			0.01	SGD	81.84
			0.0001		88.58
		16	0.001		87.67
		32			81.97
	30	16			86.25
EfficientNetB3	15	8	0.001	SGD	88.45
				ADAM	77.30
				RMSprop	85.86
			0.01	SGD	66.40
			0.0001		61.69
		16	0.001		86.51
		32			88.97
	30	16			84.69

Skin Cancer

The data were divided according to Table 3.13, and the results represented in Table 3.14 were obtained:

Table 3.13: Skin Cancer dataset Split

Label Names	**Train Count**	**Validation Count**	**Test Count**
benign	1152	288	360
malignant	957	240	300
Total Image Count	**2109**	**528**	**660**

Table 3.14: The results for Skin Cancer dataset

MODEL	EPOCH	BATCH SIZE	LAR RATE	OPTEM	TEST ACC
ResNet50	15	8	0.001	SGD	90.15
				ADAM	82.87
				RMSprop	83.33
			0.01	SGD	82.87
			0.0001		87.87
		16	0.001		90.0
		32			88.18
	30	8			91.30
DenseNet-121	15	8	0.001	SGD	88.18
				ADAM	86.06
				RMSprop	83.93
			0.01	SGD	83.33
			0.001		83.48
		16	0.001		87.72
		32			85.90
	30	8			88.18
EfficientNetB3	15	8	0.001	SGD	89.09
				ADAM	83.78
				RMSprop	84.09
			0.01	SGD	82.57
			0.0001		88.18
		16	0.001		90.30
		32			89.54
	30	16			89.09

Kvasir Dataset

The data were divided according to Table 3.15, and the results represented in Table 3.16 were obtained:

Table 3.15: Kvasir Dataset Split

Label Names	**Train Count**	**Validation Count**	**Test Count**
dyed-lifted-polyps	400	50	50
dyed-resection-margins	400	50	50
esophagitis	400	50	50
normal-cecum	400	50	50
normal-pylorus	400	50	50
normal-z-line	400	50	50
polyps	400	50	50
ulcerative-colitis	400	50	50
Total Image Count	**3200**	**400**	**400**

Table 3.16: The results for Kvasir Dataset

MODEL	EPOCH	BATCH SIZE	LAR RATE	OPTEM	TEST ACC
ResNet50	15	8	0.001	SGD	94.52
				ADAM	67.5
				RMSprop	67
			0.01	SGD	77
			0.0001		92.75
		16	0.001		92.75
		32			94
	30	32			93.5
DenseNet-121	15	8	0.001	SGD	92 .5
				ADAM	85.5
				RMSprop	75.61
			0.01	SGD	75.75
			0.0001		91.25
		16	0.001		93.5
		32			91.75
	30	16			92.75
EfficientNetB3	15	8	0.001	SGD	92.5
				ADAM	82.25
				RMSprop	78.5
			0.01	SGD	67
			0.0001		87
		16	0.001		91
		32			75 .25
	30	16			92.25

3.3.2 Testing with Data Augmentation

In the second part, we concentrated on perfecting the variables that each dataset's best accuracy required. To further improve the performance of our model, we also used a number of data augmentation approaches. The diversity and volume of the training data can be artificially increased by the use of these augmentation approaches, which can enhance the generalization and robustness of the model.

- Rotation with 90 degrees
- Horizontal and Vertical Flip
- Brightness=0.4
- Contrast=0.4
- saturation=0.4
- hue=0.1

Brain Tumor MRI

Figure 3.6 presents a collection of images from the dataset that have undergone the data augmentation techniques described earlier. These augmented images vividly illustrate the transformative impact of the augmentation process on the visual characteristics and diversity of the training data.

We applied this method to the parameters that got the best accuracy (model=DenseNet-121, 15 epochs, batch size =8, learning rate = 0.001, and optimizer = SGD) from part one, tables 3.17 and 3.18, and Fig. 3.7 and 3.8, represent the obtained results.

Table 3.17: The results with data augmentation for Brain Tumor MRI

Dataset	**Resize**	**Color Jitter**	**Resize, Color Jitter, Rotation**	**Resize, Color Jitter, Rotation, Flip**
Brain	99.43%	**99.43%**	99.14%	99.007%

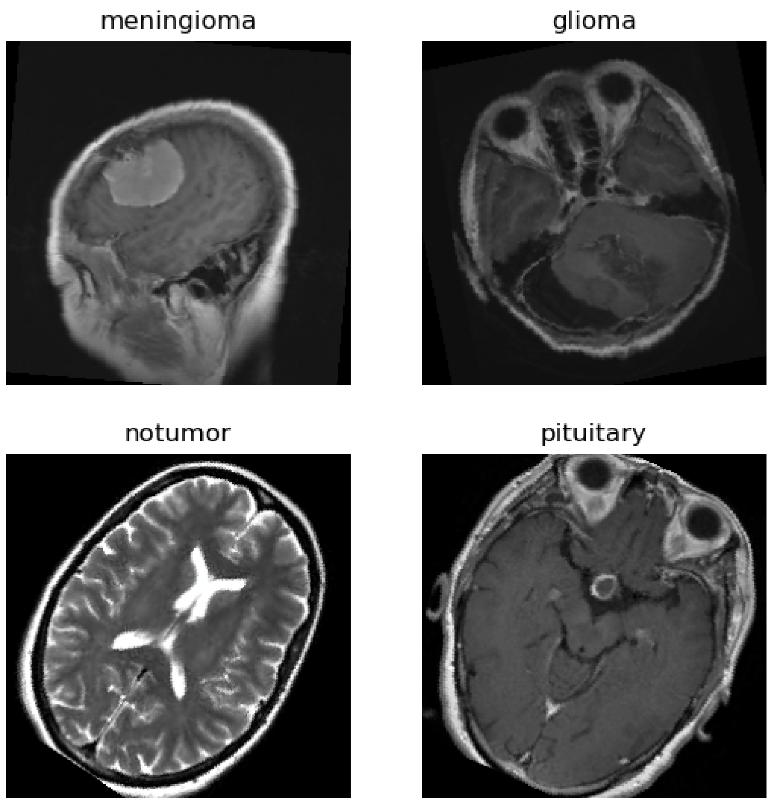

Figure 3.6: Images from the Brain dataset after data augmentation

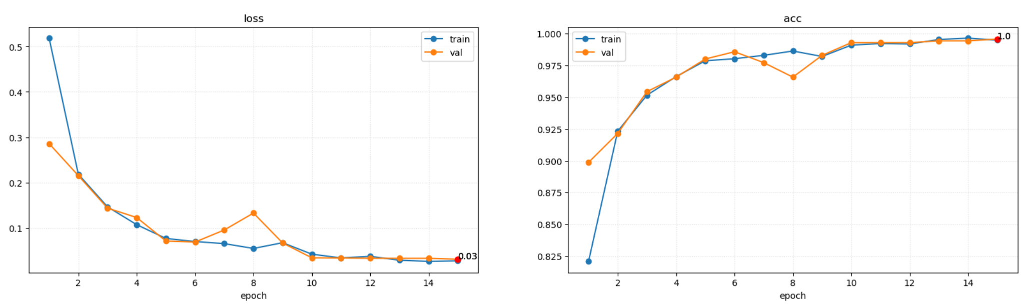

Figure 3.7: Best results: Accuracies (training validation)

Table 3.18: The classification report for Brain Tumor MRI

	precision	recall	f1-score	support
glioma	1.0000	1.0000	1.0000	163
meningioma	0.9879	0.9879	0.9879	165
notumor	1.0000	1.0000	1.0000	200
pituitary	0.9887	0.9887	0.9887	177
accuracy			0.9943	705
macro avg	0.9941	0.9941	0.9941	705
weighted avg	0.9943	0.9943	0.9943	705

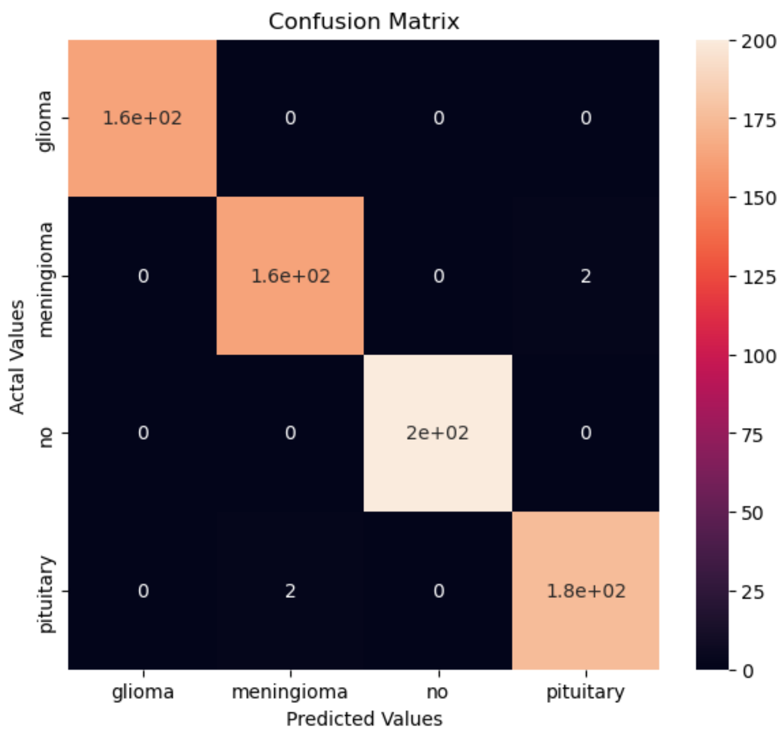

Figure 3.8: Best results: Confusion matrix)

Alzheimer MRI

Figure 3.9 presents a collection of images from the dataset that have undergone the data augmentation techniques described earlier. These augmented images vividly illustrate the transformative impact of the augmentation process on the visual characteristics and diversity of the training data.

We applied this method to the parameters that got the best accuracy (model=ResNet50, 15 epochs, batch size =16, learning rate = 0.001, and optimizer = SGD) from part one, tables 3.19 and 3.20, and Fig. 3.10 and 3.11, represent the obtained results.

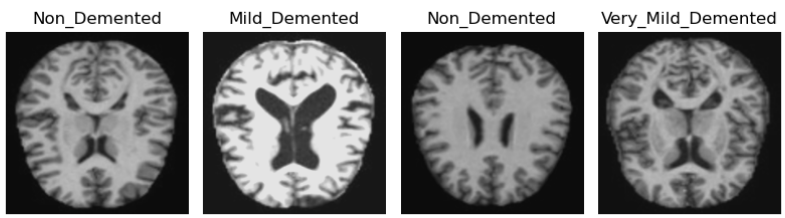

Figure 3.9: Images from the Alzheimer dataset after data augmentation

Table 3.19: The results with data augmentation for Alzheimer MRI

Dataset	**Resize**	**Color Jitter**	**Resize, Color Jitter, Rotation**	**Resize, Color Jitter, Rotation, Flip**
Alzheimer	99.53	**99.53**	97.14	98.75

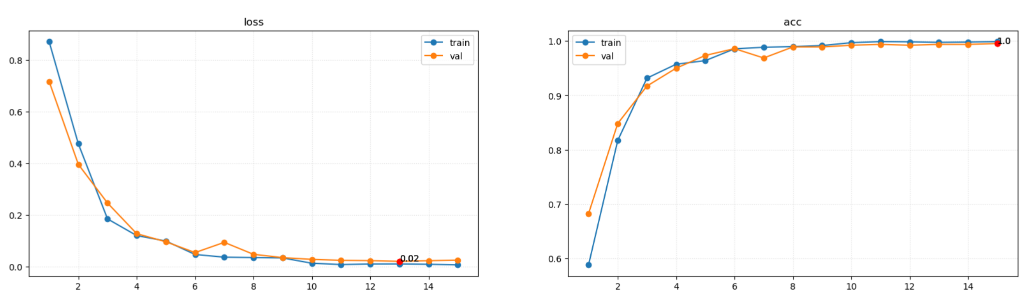

Figure 3.10: Best results: Accuracies (training validation)

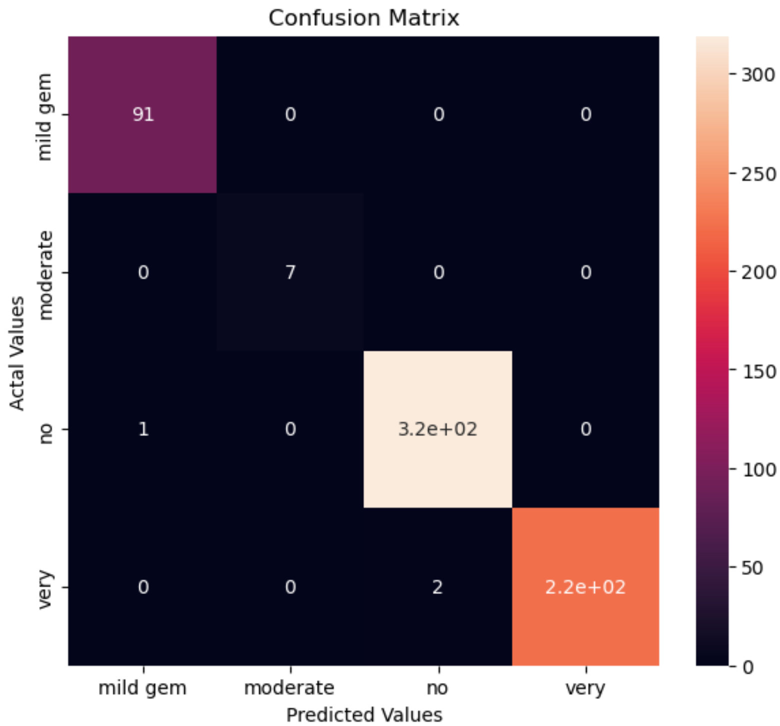

Figure 3.11: Best results: Confusion matrix)

Table 3.20: The classification report Alzheimer MRI

	precision	recall	f1-score	support
Mild$_{Demented}$	0.9891	1.0000	0.9945	91
Moderate$_{Demented}$	1.0000	1.0000	1.0000	7
Non$_{Demented}$	0.9938	0.9969	0.9953	320
Very$_{M}ild_{D}emented$	1.0000	0.9911	0.9955	224
accuracy			0.9953	642
macro avg	0.9957	0.9970	0.9963	642
weighted avg	0.9954	0.9953	0.9953	642

Chest X-Ray

Figure 3.12 presents a collection of images from the dataset that have undergone the data augmentation techniques described earlier. These augmented images vividly illustrate the transformative impact of the augmentation process on the visual characteristics and diversity of the training data.

We applied this method to the parameters that got the best accuracy (model=ResNet50, 30 epochs, batch size =8, learning rate = 0.001, and optimizer = SGD) from part one, tables 3.21 and 3.22, and Fig. 3.13 and 3.14, represent the obtained results.

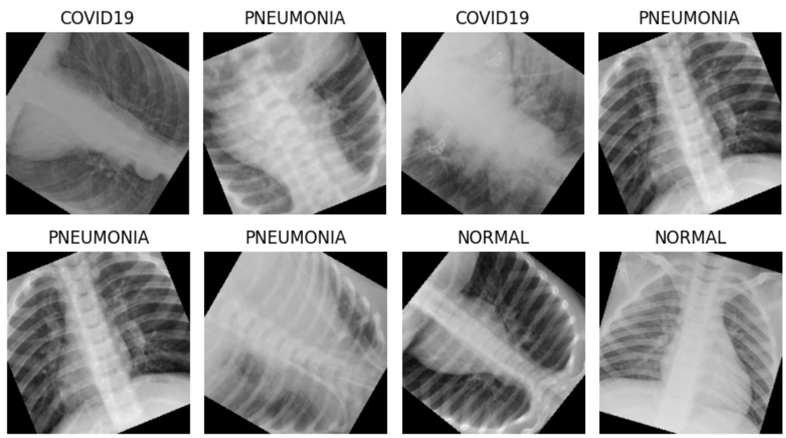

Figure 3.12: Images from the Chest X-Ray dataset after data augmentation

Table 3.21: The results with data augmentation for Chest X-Ray

Dataset	**Resize**	**Color Jitter**	**Resize, Color Jitter, Rotation**	**Resize, Color Jitter, Rotation, Flip**
Chest X-Ray	92.00	88.58	**92.21**	88.97

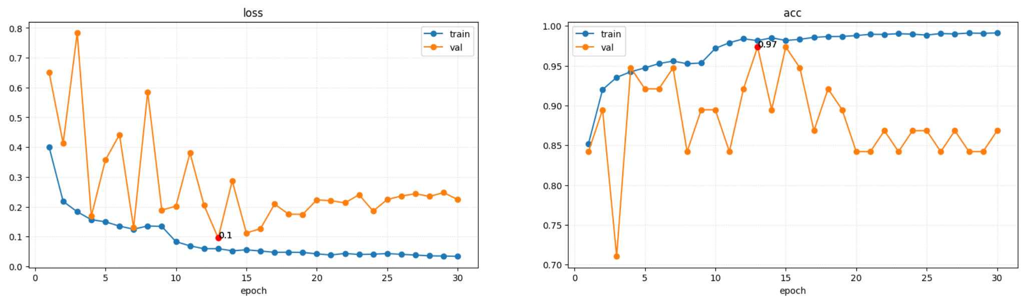

Figure 3.13: Best results: Accuracies (training validation)

Table 3.22: The classification report for Chest X-Ray

	precision	recall	f1-score	support
COVID19	0.9903	0.9623	0.9761	106
NORMAL	0.9890	0.7692	0.8654	234
PNEUMONIA	0.8818	0.9949	0.9349	390
TURBERCULOSIS	0.8913	1.0000	0.9425	41
accuracy			0.9222	771
macro avg	0.9381	0.9316	0.9297	771
weighted avg	0.9298	0.9222	0.9199	771

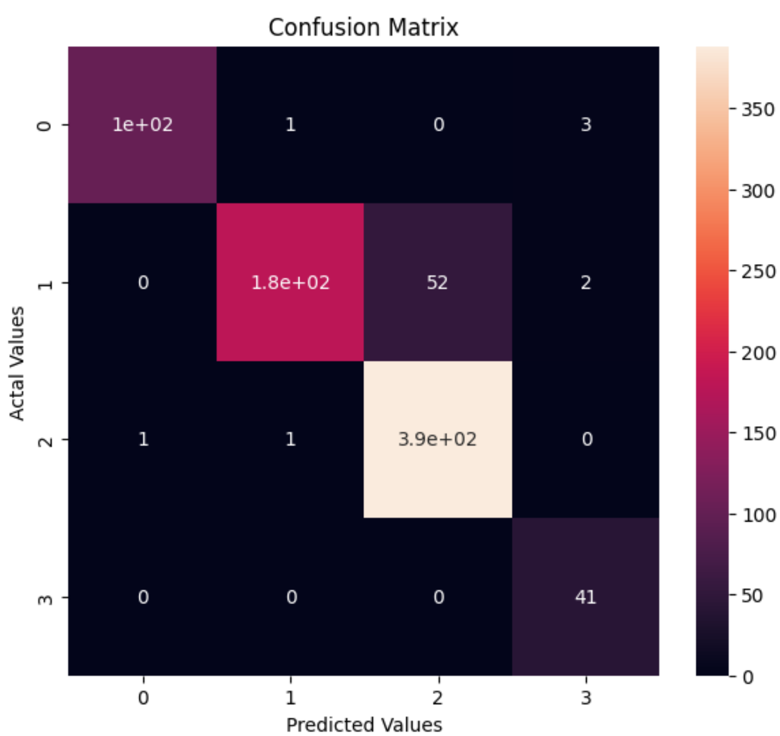

Figure 3.14: Best results: Confusion matrix)

Skin Cancer

Figure 3.15 presents a collection of images from the dataset that have undergone the data augmentation techniques described earlier. These augmented images vividly illustrate the transformative impact of the augmentation process on the visual characteristics and diversity of the training data.

We applied this method to the parameters that got the best accuracy (model=ResNet50, 30 epochs, batch size =8, learning rate = 0.001, and optimizer = SGD) from part one, tables 3.23 and 3.24, and Fig. 3.16 and 3.17, represent the obtained results.

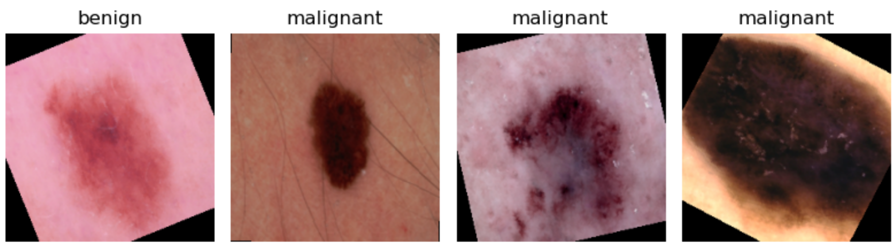

Figure 3.15: Images from the Skin Cancer dataset after data augmentation

Table 3.23: The results with data augmentation for Skin Cancer

Dataset	**Resize**	**Color Jitter**	**Resize, Color Jitter, Rotation**	**Resize, Color Jitter, Rotation, Flip**
Skin	**90.30**	87.12	87.42	85.30

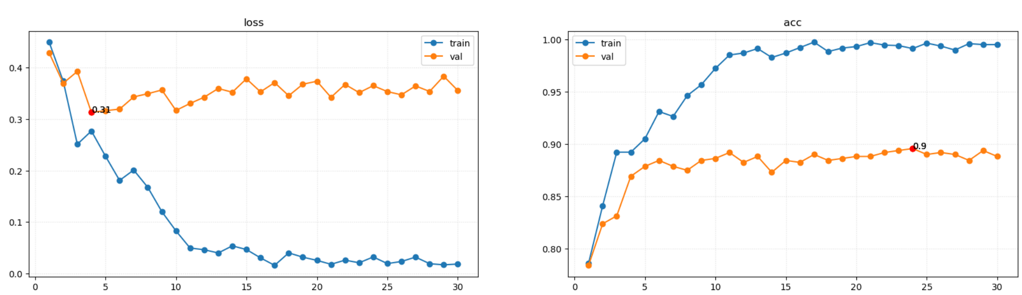

Figure 3.16: Best results: Accuracies (training validation)

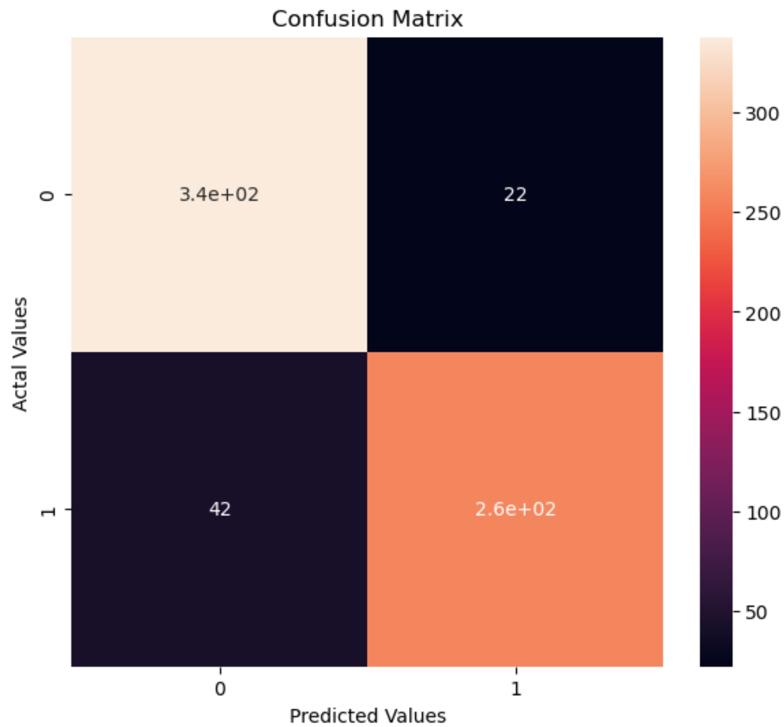

Figure 3.17: Best results: Confusion matrix)

Table 3.24: The classification report for Skin Cancer

	precision	recall	f1-score	support
benign	0.8895	0.9389	0.9135	360
malignant	0.9214	0.8600	0.8897	300
accuracy			0.9030	660
macro avg	0.9055	0.8994	0.9016	660
weighted avg	0.9040	0.9030	0.9027	660

Kvasir Dataset

Figure 3.18 presents a collection of images from the dataset that have undergone the data augmentation techniques described earlier. These augmented images vividly illustrate the transformative impact of the augmentation process on the visual characteristics and diversity of the training data.

We applied this method to the parameters that got the best accuracy (model=ResNet50, 15 epochs, batch size =8, learning rate = 0.001, and optimizer = SGD) from part one, tables 3.25 and 3.26, and Fig. 3.19 and 3.20, represent the obtained results.

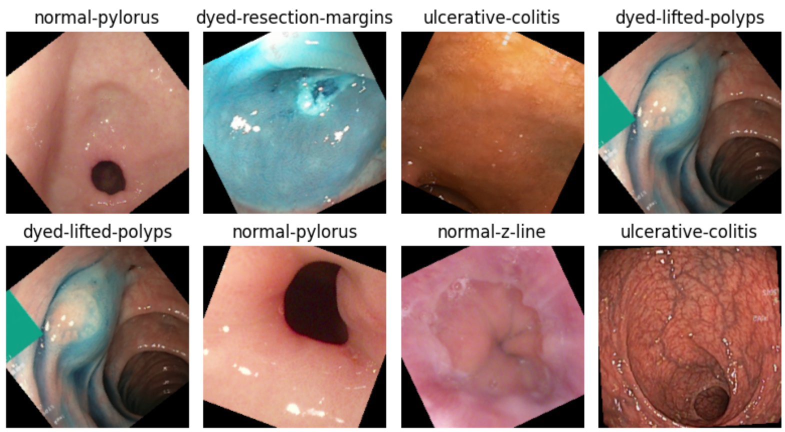

Figure 3.18: Images from the Kvasir dataset after data augmentation

Table 3.25: The results with data augmentation for Kvasir Dataset

Dataset	**Resize**	**Color Jitter**	**Resize, Color Jitter, Rotation**	**Resize, Color Jitter, Rotation, Flip**
Kvasir	94.52	93	94.5	**95**

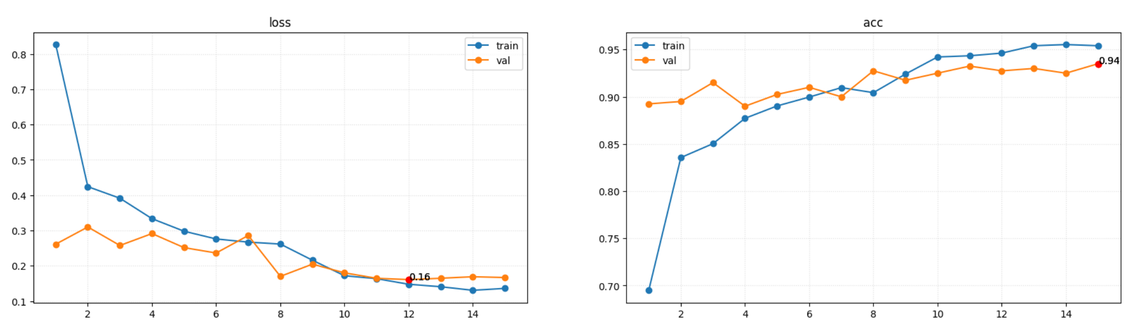

Figure 3.19: Best results: Accuracies (training validation)

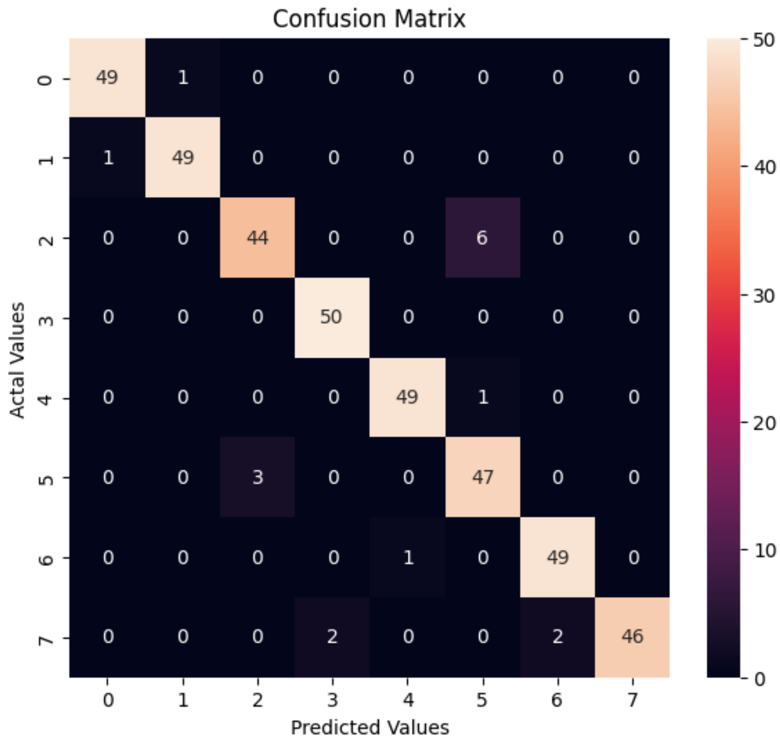

Figure 3.20: Best results: Confusion matrix)

Table 3.26: The classification report for Kvasir Dataset

	precision	recall	f1-score	support
dyed-lifted-polyps	0.9434	1.0000	0.9709	50
dyed-resection-margins	1.0000	0.9400	0.9691	50
esophagitis	0.8936	0.8400	0.8660	50
normal-cecum	0.9615	1.0000	0.9804	50
normal-pylorus	0.9804	1.0000	0.9901	50
normal-z-line	0.8654	0.9000	0.8824	50
polyps	0.9796	0.9600	0.9697	50
ulcerative-colitis	0.9796	0.9600	0.9697	50
accuracy			0.9500	400
macro avg	0.9504	0.9500	0.9498	400
weighted avg	0.9504	0.9500	0.9498	400

3.3.3 Comparative Study

A summary of the results obtained and comparison with other studies that worked on the same datasets that we used are represented in the following table 3.27:

Table 3.27: Comparison with state-of-the-art methods

Reference	**Dataset**	**Method**	**Test accuracy (%)**
Perpossed Uysal et al. [96]	Brain Tumor MRI	EfficientNet-B3 ResNet50	99.43 99.43
Perpossed Sekhar and Jagadev [97]	Alzheimer MRI	ResNet50 CNN-based efficientnet	99.53 98.0
Perpossed Hamza et al. [98]	Chest X-Ray	ResNet50 CSVM classifier	92.21 98.3
Perpossed Anand et al. [99]	Skin Cancer	ResNet50 Modified VGG16	90.30 89.09
Perpossed Khan et al. [80]	Kvasir	ResNet50 GestroNet	95.00 98.20

3.4 application

The "My Daily Health" app was developed with the Tinkter library with the goal of assisting you in tracking your daily health and enhancing your way of life. This program offers customers a user-friendly and effective graphical user interface (GUI) for monitoring and documenting their health information.

Login page

After run the application, the main page shows, contain on entry for the username and the password and two button for login in your account or register a new one.

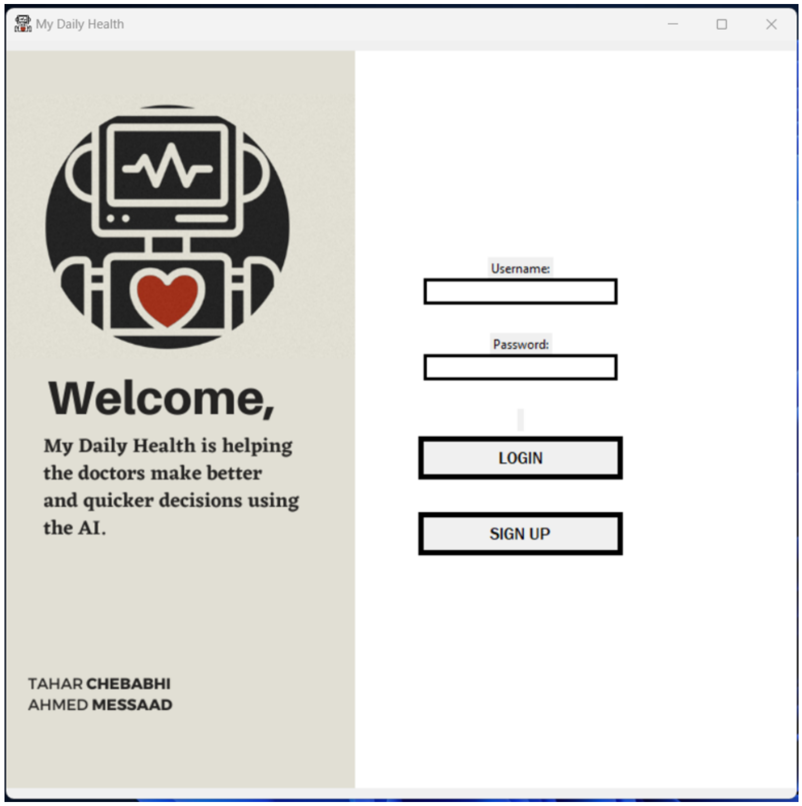

Figure 3.21: Login page

Main page Main page : After login, in this page there are a three buttons: Start button: to begin the image diagnostic.

History: the history of patient.

Logout: logout from the account

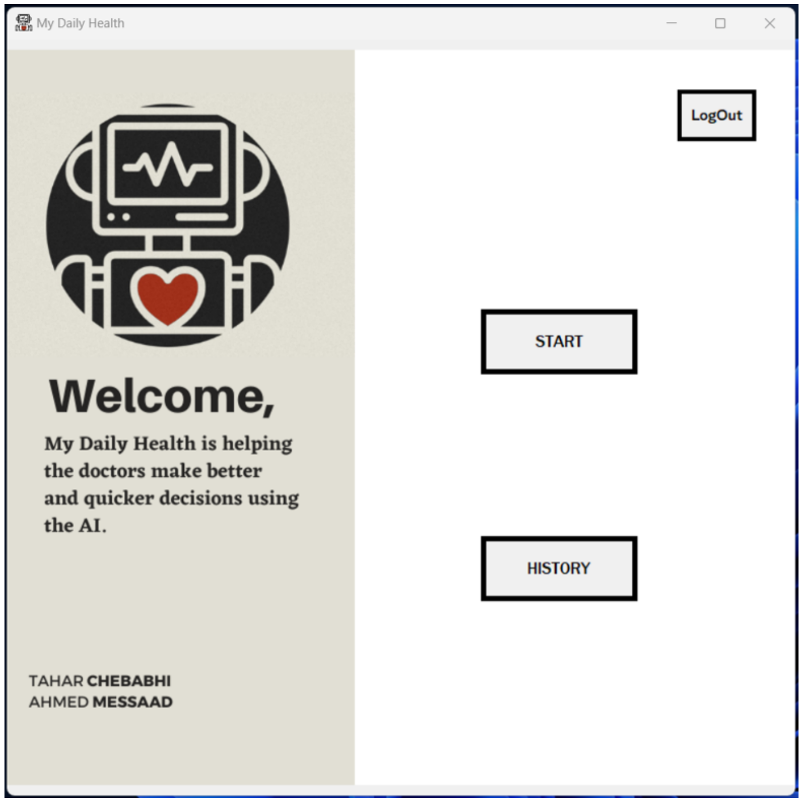

Figure 3.22: Main page

Select types page Select types page : In this page the user select the types of the image disease.

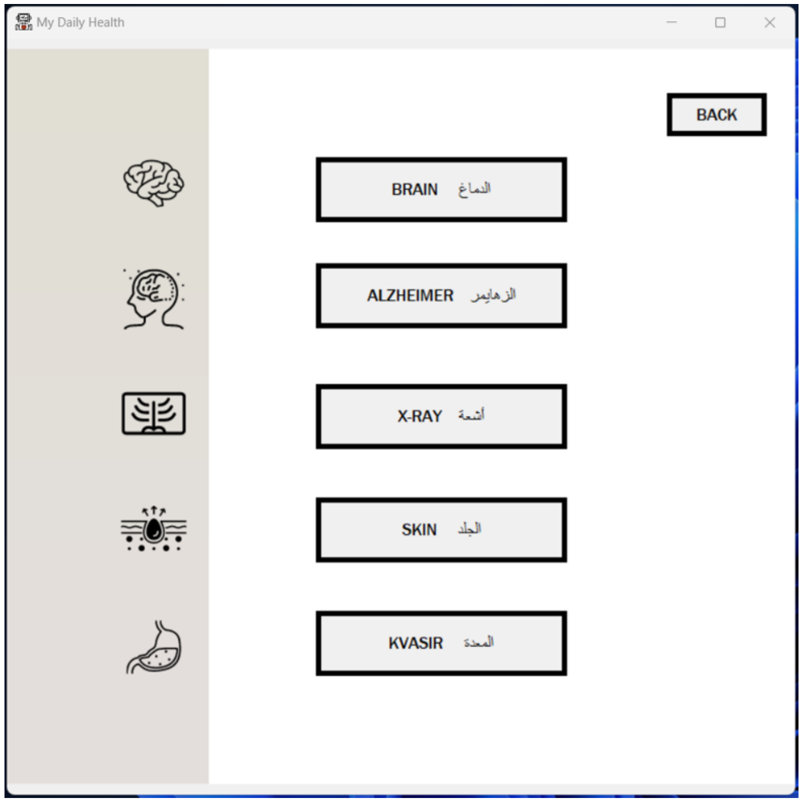

Figure 3.23: Select types page

Upload page Upload page : After selecting the type of image disease, now Choose the image to be diagnosed.

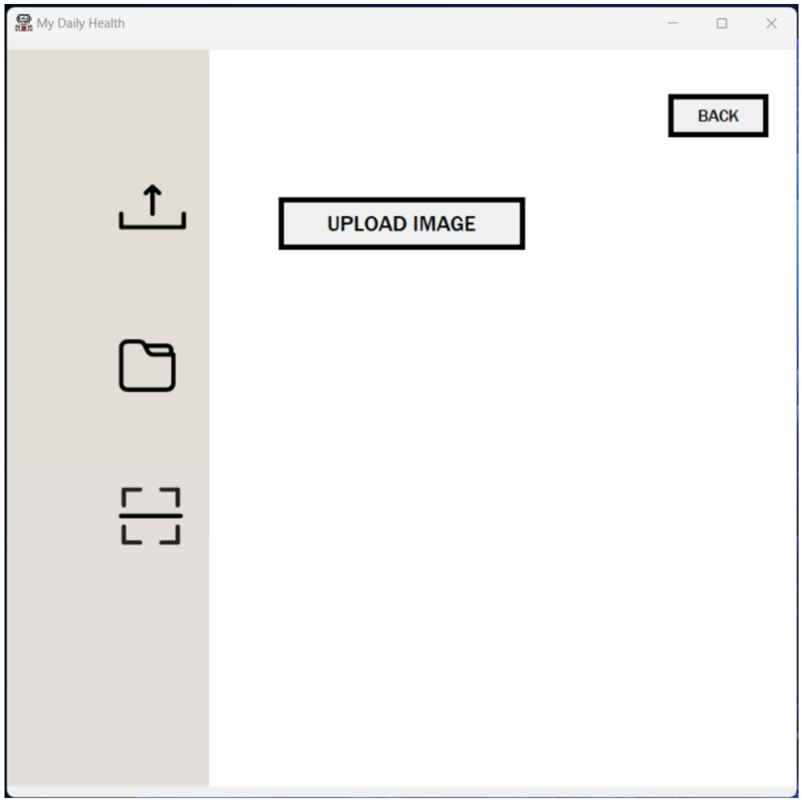

Figure 3.24: Upload page

Result page Result page: the result of the diagnosed image shown with the disease types is represented by the percentage of each type. The larger value is in red. There is also a field for writing the medical report or notes about the image or the patient, which can be saved with the save button.also a Logout button to start from the beginning.

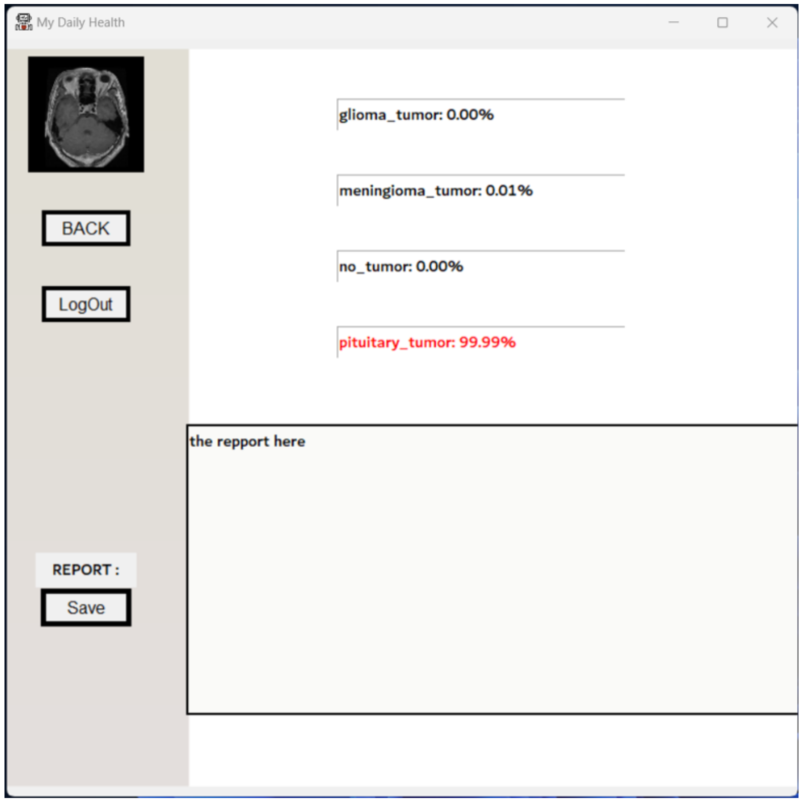

Figure 3.25: Result page

History page History page In this page, all the previous reports of patient shown, from the Result page.

This page can access from the button History in the main page

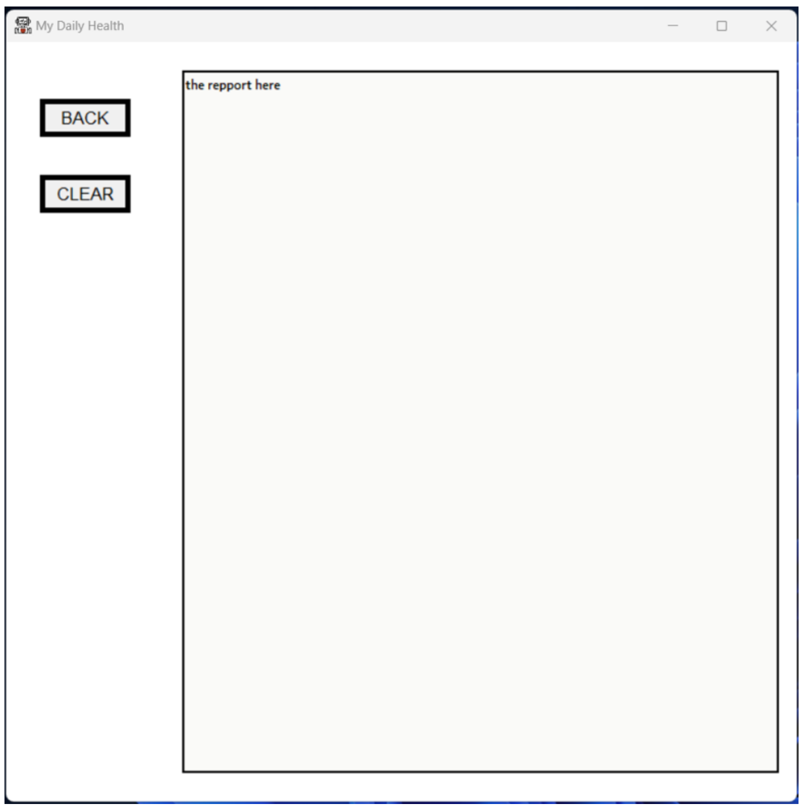

Figure 3.26: History page

CONCLUSION GENERAL

The use of AI techniques, specifically deep learning and transfer learning, has ushered in a new era of improvements in illness diagnosis, treatment planning, and patient monitoring. Biomedical data, such as MRI, X-ray, PET, CT images, and microscopic images, provides valuable insights into physiological and pathological processes. AI has emerged as a powerful tool for processing and analyzing large amounts of data, identifying patterns, and making predictions.

Deep transfer learning, a powerful approach in deep learning, has revolutionized biomedical data analysis by uncovering complex patterns in biomedical images. It applies knowledge from pre-trained models to improve the performance and efficiency of disease analysis in various conditions such as brain tumors, Alzheimer's, respiratory illnesses, skin cancer, and gastrointestinal illnesses.

The study highlights the effectiveness of modern methods like ResNet50, DenseNet-121, and EfficientNet-B3, along with the importance of data augmentation strategies.

Overall, deep transfer learning has the potential to enhance diagnostic accuracy, support clinical decision-making, and improve patient care, offering valuable insights for more precise disease analysis and shaping the future of healthcare.

Further research and development are needed as the area continues to advance in order to solve issues with data quality, the interpretability of AI models, and ethical considerations. However, the combination of AI with biological data analysis presents a paradigm shift that has the potential to change healthcare by enabling researchers and clinicians to make better decisions and enhance patient outcomes.

Bibliography

[1] Adam Bohr and Kaveh Memarzadeh. The rise of artificial intelligence in healthcare applications. In *Artificial Intelligence in healthcare*, pages 25–60. Elsevier, 2020.

[2] Mohammad Mustafa Taye. Understanding of machine learning with deep learning: Architectures, workflow, applications and future directions. *Computers*, 12(5):91, 2023.

[3] Edward H Shortliffe and Michael F Chiang. Biomedical data: Their acquisition, storage, and use. In *Biomedical Informatics: Computer Applications in Health Care and Biomedicine*, pages 45–75. Springer International Publishing, Cham, 2021.

[4] Shuang Wang, M Emre Celebi, Yong Dou Zhang, Xiaoyang Yu, Shuai Lu, Xiaohong Yao, ..., and Ivan Tyukin. Advances in data preprocessing for biomedical data fusion: an overview of the methods, challenges, and prospects. *Information Fusion*, 76:376–421, 2021.

[5] Girish Katti, Shahina Akhtar Ara, and Afshan Shireen. Magnetic resonance imaging (mri)–a review. *International Journal of Dental Clinics*, 3(1):65–70, 2011.

[6] Johns Hopkins Medicine. X-rays. https://www.hopkinsmedicine.org/health/treatment-tests-and-therapies/xrays, n.d. Accessed on April 2, 2023.

[7] Yen F Tai and Paola Piccini. Applications of positron emission tomography (pet) in neurology. *Journal of Neurology, Neurosurgery & Psychiatry*, 75(5):669–676, 2004.

[8] Daniel T Ginat and Rajiv Gupta. Advances in computed tomography imaging technology. *Annual review of biomedical engineering*, 16:431–453, 2014.

[9] Michalis Mazonakis and John Damilakis. Computed tomography: What and how does it measure? *European journal of radiology*, 85(8):1499–1504, 2016.

[10] Nidhi Thakur and Monica Juneja. Pre-processing of retinal images acquired from digital fundus cameras for improved performance of diagnostic tools in biomedical engineering. *Materials Today: Proceedings*, 28:1525–1529, 2020.

[11] FDA. Ultrasound imaging — fda. https://www.fda.gov/radiation-emitting-products/medical-maging/ultrasound-imaging: :text=Ultrasound2022. Accessed on June 16, 2022.

[12] NHS. Endoscopy. https://www.nhs.uk/conditions/endoscopy/: :text=Ann.d. Accessed on June 16, 2022.

[13] Radiological Society of North America (RSNA) and American College of Radiology (ACR). Elastography. https://www.radiologyinfo.org/en/info/elastography: :text=Elastography2022. Accessed on June 16, 2022.

[14] Joel Schuett. A legal definition of ai. *arXiv preprint arXiv:1909.01095*, 2019.

[15] Hsin-Yuan Chiu, Hsiang-Sheng Chao, and Yu-Ming Chen. Application of artificial intelligence in lung cancer. *Cancers*, 14(6):1370, 2022.

[16] Nick Bostrom. *Superintelligence: Paths, Dangers, Strategies*. Oxford University Press, 2014.

[17] Stuart Russell and Peter Norvig. *Artificial Intelligence: A Modern Approach*. Pearson, 2010.

[18] Pavel Hamet and Johanne Tremblay. Artificial intelligence in medicine. *Metabolism*, 69(Supplement):S36–S40, 2017.

[19] Xiaoyang Wang, Yifei Zhao, and Farshad Pourpanah. Recent advances in deep learning. *Int. J. Mach. Learn. & Cyber.*, 11:747–750, 2020.

[20] Anu Mathew, P Amudha, and S Sivakumari. Deep learning techniques: An overview. In *Advanced Machine Learning Technologies and Applications*, volume 1141 of *Advances in Intelligent Systems and Computing*, pages 617–630. Springer, 2021.

[21] Jaya Koushik. Understanding convolutional neural networks. *arXiv preprint arXiv:1605.09081*, 2016.

[22] Chuanqi Tan, Fuchun Sun, Tao Kong, Wenchang Zhang, Chao Yang, and Chunfang Liu. A survey on deep transfer learning. In *Artificial Neural Networks and Machine Learning–ICANN 2018*, pages 270–279. Springer, 2018.

[23] Simplilearn. Top 10 deep learning algorithms you should know in 2023. https://www.simplilearn.com/tutorials/deep-learning-tutorial/deep-learning-algorithm. Accessed on April 3, 2023.

[24] Rafael Ribani and Mauricio Marengoni. A survey of transfer learning for convolutional neural networks. In *2019 32nd SIBGRAPI Conference on Graphics, Patterns and Images Tutorials (SIBGRAPI-T)*, pages 47–57, 2019.

[25] Dianne Castillo. Transfer learning for machine learning, Jun 2021.

[26] A. Shatnawi, G. Al-Bdour, R. Al-Qurran, and M. Al-Ayyoub. A comparative study of open source deep learning frameworks. In *2018 9th International Conference on Information and Communication Systems (ICICS)*, pages 72–77, 2018.

[27] Why pytorch is the deep learning framework of the future$_2019, Oct$2019.

[28] Karen Simonyan and Andrew Zisserman. Very deep convolutional networks for large-scale image recognition. *arXiv preprint arXiv:1409.1556*, 2014.

[29] Kaiming He, Xiangyu Zhang, Shaoqing Ren, and Jian Sun. Identity mappings in deep residual networks. In *Computer Vision–ECCV 2016: 14th European Conference*, pages 630–645. Springer International Publishing, October 2016.

[30] Sejuti Das. Gpt-3 vs bert for nlp tasks, Sep 2020.

[31] Ayush Gupta. A comprehensive guide on optimizers in deep learning, Oct 2021.

[32] Brain tumor - symptoms and causes. Mayo Clinic, April 2023.

[33] Shamsan Z. Kurdi, Muhammad H. Ali, Maram M. Jaber, Tanzila Saba, Atiq Rehman, and Robertas Damaševičius. Brain tumor classification using meta-heuristic optimized convolutional neural networks. *Journal of Personalized Medicine*, 13(2):181, 2023.

[34] Mohammad M. Mijwil, Ravi Doshi, Kumar K. Hiran, Ocholi J. Unogwu, and Ibrahim Bala. Mobilenetv1-based deep learning model for accurate brain tumor classification. *Mesopotamian Journal of Computer Science*, 2023:32–41, 2023.

[35] Emrah Irmak. Multi-classification of brain tumor mri images using deep convolutional neural network with fully optimized framework. *Iranian Journal of Science and Technology, Transactions of Electrical Engineering*, 45(3):1015–1036, 2021.

[36] Khushboo Munir, Fabrizio Frezza, and Antonello Rizzi. Brain tumor segmentation using 2d-unet convolutional neural network. *Deep Learning for Cancer Diagnosis*, pages 239–248, 2021.

[37] Erena Siyoum Biratu, Friedhelm Schwenker, Taye Girma Debelee, Samuel Rahimeto Kebede, Worku Gachena Negera, and Hasset Tamirat Molla. Enhanced region growing for brain tumor mr image segmentation. *Journal of Imaging*, 7(2):22, 2021.

[38] Prabhjot Kaur Chahal and Shreelekha Pandey. A hybrid weighted fuzzy approach for brain tumor segmentation using mr images. *Neural Computing and Applications*, pages 1–15, 2021.

[39] Sarmad Maqsood, Robertas Damaševičius, and Rytis Maskeliūnas. Multi-modal brain tumor detection using deep neural network and multiclass svm. *Medicina*, 58(8):1090, 2022.

[40] Venkatesan Rajinikanth, Seifedine Kadry, Robertas Damaševičius, R Angel Sujitha, Gangadharam Balaji, and Mazin Abed Mohammed. Glioma/glioblastoma detection in brain mri using pre-trained deep-learning scheme. In *2022 Third International Conference on Intelligent Computing Instrumentation and Control Technologies (ICICICT)*, pages 987–990. IEEE, 2022.

[41] Bakary Badjie and Ezgi Deniz Ülker. A deep transfer learning based architecture for brain tumor classification using mr images. *Information Technology and Control*, 51(2):332–344, 2022.

[42] Muhannad Faleh Alanazi, Muhammad Umair Ali, Shaik Javeed Hussain, Amad Zafar, Mohammed Mohatram, Muhammad Irfan, Raed AlRuwaili, Mubarak Alruwaili, Naif H Ali, and Anas Mohammad Albarrak. Brain tumor/mass classification framework using magnetic-resonance-imaging-based isolated and developed transfer deep-learning model. *Sensors*, 22(1):372, 2022.

[43] Usman Zahid, Imran Ashraf, Muhammad Attique Khan, Majed Alhaisoni, Khawaja M Yahya, Hany S Hussein, and Hammam Alshazly. Brainnet: optimal deep learning feature fusion for brain tumor classification. *Computational Intelligence and Neuroscience*, 2022, 2022.

[44] What is alzheimer's? Alzheimer's Association. Retrieved from https://alz.org/alzheimers-dementia/what-is-alzheimers.

[45] Cucun Very Angkoso, Hapsari Peni Agustin Tjahyaningtijas, MH Purnomo, and IKE Purnama. Multiplane convolutional neural network (mp-cnn) for alzheimer's disease classification. *International Journal of Intelligent Engineering and Systems*, 15(1):329–340, 2022.

[46] Luca Heising and Spyros Angelopoulos. Operationalising fairness in medical ai adoption: detection of early alzheimer's disease with 2d cnn. *BMJ Health & Care Informatics*, 29(1), 2022.

[47] Muhammad Wildan Oktavian, Novanto Yudistira, and Achmad Ridok. Classification of alzheimer's disease using the convolutional neural network (cnn) with transfer learning and weighted loss. *arXiv preprint arXiv:2207.01584*, 2022.

[48] Modupe Odusami, Rytis Maskeliūnas, and Robertas Damaševičius. An intelligent system for early recognition of alzheimer's disease using neuroimaging. *Sensors*, 22(3):740, 2022.

[49] Modupe Odusami, Rytis Maskeliūnas, Robertas Damaševičius, and Sanjay Misra. Resd hybrid model based on resnet18 and densenet121 for early alzheimer disease classification. In *Intelligent Systems Design and Applications: 21st International Conference on Intelligent Systems Design and Applications (ISDA 2021) Held During December 13–15, 2021*, pages 296–305. Springer, 2022.

[50] Modupe Odusami, Rytis Maskeliunas, Robertas Damaševičius, and Sanjay Misra. Comparable study of pre-trained model on alzheimer disease classification. In *Computational Science and Its Applications–ICCSA 2021: 21st International Conference, Cagliari, Italy, September 13–16, 2021, Proceedings, Part V 21*, pages 63–74. Springer, 2021.

[51] N Deepa and SP Chokkalingam. Optimization of vgg16 utilizing the arithmetic optimization algorithm for early detection of alzheimer's disease. *Biomedical Signal Processing and Control*, 74:103455, 2022.

[52] Priyam Pandey, Ashish Khare, and Prashant Srivastava. Detection of alzheimer's disease using cnn architectures. *ADBU Journal of Engineering Technology*, 11(1), 2022.

[53] Avinash Bhagat, Syed Immamul Ansarullah, Mohamed Tahar Ben Othman, Yasir Hamid, Hend Khalid Alkahtani, Inam Ullah, Habib Hamam, et al. A novel framework for classification of different alzheimer's disease stages using cnn model. *Electronics*, 12(2):469, 2023.

[54] Xin Xing, Muhammad Usman Rafique, Gongbo Liang, Hunter Blanton, Yu Zhang, Chris Wang, Nathan Jacobs, and Ai-Ling Lin. Efficient training on alzheimer's disease diagnosis with learnable weighted pooling for 3d pet brain image classification. *Electronics*, 12(2):467, 2023.

[55] Lung diseases overview. WebMD, December 2022.

[56] Ferhat Ucar and Deniz Korkmaz. Covidiagnosis-net: Deep bayes-squeezenet based diagnosis of the coronavirus disease 2019 (covid-19) from x-ray images. *Medical hypotheses*, 140:109761, 2020.

[57] Abdul Waheed, Muskan Goyal, Deepak Gupta, Ashish Khanna, Fadi Al-Turjman, and Plácido Rogerio Pinheiro. Covidgan: data augmentation using auxiliary classifier gan for improved covid-19 detection. *Ieee Access*, 8:91916–91923, 2020.

[58] Jun Chen, Lianlian Wu, Jun Zhang, Liang Zhang, Dexin Gong, Yilin Zhao, Qiuxiang Chen, Shulan Huang, Ming Yang, Xiao Yang, et al. Deep learning-based model for detecting 2019 novel coronavirus pneumonia on high-resolution computed tomography. *Scientific reports*, 10(1):19196, 2020.

[59] Linda Wang, Zhong Qiu Lin, and Alexander Wong. Covid-net: A tailored deep convolutional neural network design for detection of covid-19 cases from chest x-ray images. *Scientific reports*, 10(1):1–12, 2020.

[60] Jun Wang, Yiming Bao, Yaofeng Wen, Hongbing Lu, Hu Luo, Yunfei Xiang, Xiaoming Li, Chen Liu, and Dahong Qian. Prior-attention residual learning for more discriminative covid-19 screening in ct images. *IEEE transactions on medical imaging*, 39(8):2572–2583, 2020.

[61] Ying Song, Shuangjia Zheng, Liang Li, Xiang Zhang, Xiaodong Zhang, Ziwang Huang, Jianwen Chen, Ruixuan Wang, Huiying Zhao, Yutian Chong, et al. Deep learning enables accurate diagnosis of novel coronavirus (covid-19) with ct images. *IEEE/ACM transactions on computational biology and bioinformatics*, 18(6):2775–2780, 2021.

[62] Erdi Acar, Engin Şahin, and İhsan Yılmaz. Improving effectiveness of different deep learning-based models for detecting covid-19 from computed tomography (ct) images. *Neural Computing and Applications*, 33(24):17589–17609, 2021.

[63] Shaoping Hu, Yuan Gao, Zhangming Niu, Yinghui Jiang, Lao Li, Xianglu Xiao, Minhao Wang, Evandro Fei Fang, Wade Menpes-Smith, Jun Xia, et al. Weakly supervised deep learning for covid-19 infection detection and classification from ct images. *IEEE Access*, 8:118869–118883, 2020.

[64] Xinggang Wang, Xianbo Deng, Qing Fu, Qiang Zhou, Jiapei Feng, Hui Ma, Wenyu Liu, and Chuansheng Zheng. A weakly-supervised framework for covid-19 classification and lesion localization from chest ct. *IEEE transactions on medical imaging*, 39(8):2615–2625, 2020.

[65] Editors of Encyclopaedia Britannica. Skin cancer. Encyclopedia Britannica, April 2023.

[66] Shilpa Saravanan, B Heshma, AV Ashma Shanofer, and R Vanithamani. Skin cancer detection using dermoscope images. *Materials Today: Proceedings*, 33:4823–4827, 2020.

[67] Ahmed Refaat Hawas, Yanhui Guo, Chunlai Du, Kemal Polat, and Amira S Ashour. Oce-ngc: A neutrosophic graph cut algorithm using optimized clustering estimation algorithm for dermoscopic skin lesion segmentation. *Applied Soft Computing*, 86:105931, 2020.

[68] Şaban Öztürk and Umut Özkaya. Skin lesion segmentation with improved convolutional neural network. *Journal of digital imaging*, 33:958–970, 2020.

[69] Cheng Huang, Anyuan Yu, Yiwen Wang, and Honglin He. Skin lesion segmentation based on mask r-cnn. In *2020 International Conference on Virtual Reality and Visualization (ICVRV)*, pages 63–67. IEEE, 2020.

[70] Pufang Shan, Yiding Wang, Chong Fu, Wei Song, and Junxin Chen. Automatic skin lesion segmentation based on fc-dpn. *Computers in Biology and Medicine*, 123:103762, 2020.

[71] Amira S Ashour, Reham Mohamed Nagieb, Heba A El-Khobby, Mustafa M Abd Elnaby, and Nilanjan Dey. Genetic algorithm-based initial contour optimization for skin lesion border detection. *Multimedia Tools and Applications*, 80:2583–2597, 2021.

[72] Ranpreet Kaur, Hamid GholamHosseini, Roopak Sinha, and Maria Lindén. Automatic lesion segmentation using atrous convolutional deep neural networks in dermoscopic skin cancer images. *BMC Medical Imaging*, 22(1):1–13, 2022.

[73] Rasmiranjan Mohakud and Rajashree Dash. Skin cancer image segmentation utilizing a novel en-gwo based hyper-parameter optimized fcedn. *Journal of King Saud University-Computer and Information Sciences*, 34(10):9889–9904, 2022.

[74] Angelica Bottaro. The most common gastrointestinal diseases, October 25 2022. Medically reviewed by Shadi Hamdeh, MD.

[75] J Yogapriya, Venkatesan Chandran, MG Sumithra, P Anitha, P Jenopaul, and C Suresh Gnana Dhas. Gastrointestinal tract disease classification from wireless endoscopy images using pretrained deep learning model. *Computational and mathematical methods in medicine*, 2021, 2021.

[76] Şaban Öztürk and Umut Özkaya. Gastrointestinal tract classification using improved lstm based cnn. *Multimedia Tools and Applications*, 79(39-40):28825–28840, 2020.

[77] Şaban Öztürk and Umut Özkaya. Residual lstm layered cnn for classification of gastrointestinal tract diseases. *Journal of Biomedical Informatics*, 113:103638, 2021.

[78] Amartya Dutta, Rajat Kanti Bhattacharjee, and Ferdous Ahmed Barbhuiya. Efficient detection of lesions during endoscopy. In *Pattern Recognition. ICPR International Workshops and Challenges: Virtual Event, January 10-15, 2021, Proceedings, Part VIII*, pages 315–322. Springer, 2021.

[79] Karthik Ramamurthy, Timothy Thomas George, Yash Shah, and Parasa Sasidhar. A novel multi-feature fusion method for classification of gastrointestinal diseases using endoscopy images. *Diagnostics*, 12(10):2316, 2022.

[80] Muhammad Attique Khan, Naveera Sahar, Wazir Zada Khan, Majed Alhaisoni, Usman Tariq, Muhammad H Zayyan, Ye Jin Kim, and Byoungchol Chang. Gestronet: A framework of saliency estimation and optimal deep learning features based gastrointestinal diseases detection and classification. *Diagnostics*, 12(11):2718, 2022.

[81] Muhammad Attique Khan, Khan Muhammad, Shui-Hua Wang, Shtwai Alsubai, Adel Binbusayyis, Abdullah Alqahtani, Arnab Majumdar, and Orawit Thinnukool. Gastrointestinal diseases recognition: a framework of deep neural network and improved moth-crow optimization with dcca fusion. *Human-centric Comput. Inf. Sci*, 12:25, 2022.

[82] Subhashree Mohapatra, Girish Kumar Pati, Manohar Mishra, and Tripti Swarnkar. Gastrointestinal abnormality detection and classification using empirical wavelet transform and deep convolutional neural network from endoscopic images. *Ain Shams Engineering Journal*, 14(4):101942, 2023.

[83] Yaw Afriyie, Benjamin A. Weyori, and Alex A. Opoku. Gastrointestinal tract disease recognition based on denoising capsule network. *Cogent Engineering*, 9(1):2142072, 2022.

[84] Wei Wang, Xin Yang, Xin Li, and Jinhui Tang. Convolutional-capsule network for gastrointestinal endoscopy image classification. *International Journal of Intelligent Systems*, 37(9):5796–5815, 2022.

[85] Ahsan Aziz, Muhammad Khan, Usman Tariq, Yunyoung Nam, Muhammad Nazir, Chang-Won Jeong, Reham Mostafa, and Rasha Sakr. An ensemble of optimal deep learning features for brain tumor classification. *Computers, Materials and Continua*, 69:2653–2670, 07 2021.

[86] Architecture of densenet-121. OpenGenus IQ, August 2021.

[87] Papers with code - efficientnet explained. Papers with Code. Retrieved from https://paperswithcode.com/method/efficientnet.

[88] Cem Dilmegani. What is data augmentation? techniques & examples in 2023. AI Multiple, April 2021. Updated on December 26, 2022.

[89] https://www.kaggle.com/datasets/masoudnickparvar/brain-tumor-mri-dataset.

[90] https://www.kaggle.com/datasets/sachinkumar413/alzheimer-mri-dataset.

[91] https://www.kaggle.com/datasets/jtiptj/chest-xray-pneumoniacovid19tuberculosis.

[92] https://www.kaggle.com/datasets/fanconic/skin-cancer-malignant-vs-benign.

[93] Konstantin Pogorelov, Kristin Ranheim Randel, Carsten Griwodz, Sigrun Losada Eskeland, Thomas de Lange, Dag Johansen, Concetto Spampinato, Duc-Tien Dang-Nguyen, Mathias Lux, Peter Thelin Schmidt, et al. Kvasir: A multi-class image dataset for computer aided gastrointestinal disease detection. In *Proceedings of the 8th ACM on Multimedia Systems Conference*, pages 164–169, 2017.

[94] Ron Kohavi et al. A study of cross-validation and bootstrap for accuracy estimation and model selection. In *Ijcai*, volume 14, pages 1137–1145. Montreal, Canada, 1995.

[95] Hercules Dalianis and Hercules Dalianis. Evaluation metrics and evaluation. *Clinical text mining: secondary use of electronic patient records*, pages 45–53, 2018.

[96] Fatih Uysal and Metehan Erkan. Multiclass classification of brain tumors with various deep learning models. *Engineering Proceedings*, 27(1):30, 2022.

[97] BVDS Sekhar and Alok Kumar Jagadev. Efficient alzheimer's disease detection using deep learning technique. *Soft Computing*, pages 1–8, 2023.

[98] Ameer Hamza, Muhammad Attique Khan, Shui-Hua Wang, Abdullah Alqahtani, Shtwai Alsubai, Adel Binbusayyis, Hany S Hussein, Thomas Markus Martinetz, and Hammam Alshazly. Covid-19 classification using chest x-ray images: A framework of cnn-lstm and improved max value moth flame optimization. *Frontiers in Public Health*, 10, 2022.

[99] Vatsala Anand, Sheifali Gupta, Ayman Altameem, Soumya Ranjan Nayak, Ramesh Chandra Poonia, and Abdul Khader Jilani Saudagar. An enhanced transfer learning based classification for diagnosis of skin cancer. *Diagnostics*, 12(7):1628, 2022.